UNIVERSIDADE ESTADUAL DE CAMPINAS
Instituto de Física Gleb Wataghin

MATHEUS MELO SANTOS VELLOSO

OTIMIZAÇÃO ONLINE DA ABERTURA DINÂMICA DO SIRIUS

ONLINE OPTIMIZATION OF SIRIUS DYNAMIC APERTURE

CAMPINAS
2023

MATHEUS MELO SANTOS VELLOSO

ONLINE OPTIMIZATION OF SIRIUS DYNAMIC APERTURE

OTIMIZAÇÃO ONLINE DA ABERTURA DINÂMICA DO SIRIUS

Dissertação apresentada ao Instituto de Física Gleb Wataghin da Universidade Estadual de Campinas como parte dos requisitos exigidos para a obtenção do título de MESTRE EM FÍSICA, na Área de FÍSICA.

Thesis presented to the Gleb Wataghin Institute of Physics of the University of Campinas in partial fulfillment of the requirements for the degree of MASTER IN PHYSICS, in the area of PHYSICS.

Orientadora: LIU LIN

Coorientador: ANTONIO RUBENS DE CASTRO BRITTO

ESTE TRABALHO CORRESPONDE À VERSÃO FINAL DA TESE DEFENDIDA PELO ALUNO MATHEUS MELO SANTOS VELLOSO E ORIENTADA PELO PROF. DR. LIU LIN.

CAMPINAS

2023

FICHA CATALOGRÁFICA

FOLHA DA APROVAÇÃO

Acknowledgements

Lorem ipsum dolor sit amet, consectetuer adipiscing elit. Ut purus elit, vestibulum ut, placerat ac, adipiscing vitae, felis. Curabitur dictum gravida mauris. Nam arcu libero, nonummy eget, consectetuer id, vulputate a, magna. Donec vehicula augue eu neque. Pellentesque habitant morbi tristique senectus et netus et malesuada fames ac turpis egestas. Mauris ut leo. Cras viverra metus rhoncus sem. Nulla et lectus vestibulum urna fringilla ultrices. Phasellus eu tellus sit amet tortor gravida placerat. Integer sapien est, iaculis in, pretium quis, viverra ac, nunc. Praesent eget sem vel leo ultrices bibendum. Aenean faucibus. Morbi dolor nulla, malesuada eu, pulvinar at, mollis ac, nulla. Curabitur auctor semper nulla. Donec varius orci eget risus. Duis nibh mi, congue eu, accumsan eleifend, sagittis quis, diam. Duis eget orci sit amet orci dignissim rutrum.

Resumo

Lorem ipsum dolor sit amet, consectetuer adipiscing elit. Ut purus elit, vestibulum ut, placerat ac, adipiscing vitae, felis. Curabitur dictum gravida mauris. Nam arcu libero, nonummy eget, consectetuer id, vulputate a, magna. Donec vehicula augue eu neque. Pellentesque habitant morbi tristique senectus et netus et malesuada fames ac turpis egestas. Mauris ut leo. Cras viverra metus rhoncus sem. Nulla et lectus vestibulum urna fringilla ultrices. Phasellus eu tellus sit amet tortor gravida placerat. Integer sapien est, iaculis in, pretium quis, viverra ac, nunc. Praesent eget sem vel leo ultrices bibendum. Aenean faucibus. Morbi dolor nulla, malesuada eu, pulvinar at, mollis ac, nulla. Curabitur auctor semper nulla. Donec varius orci eget risus. Duis nibh mi, congue eu, accumsan eleifend, sagittis quis, diam. Duis eget orci sit amet orci dignissim rutrum.

Abstract

Beam accumulation into the SIRIUS storage ring occurs in the off-axis scheme, for which the efficiency depends on a sufficiently large dynamic aperture (DA) - the region comprising stable transverse oscillations. In the design phase, SIRIUS DA was numerically optimized in the accelerator model using various techniques and during commissioning the optimized lattice was implemented in the machine. Recent measurements indicate that SIRIUS DA, although sufficiently large for an injection efficiency of around 85%, can be yet increased upon fine-tuning of sextupole magnets strengths, which govern the beam nonlinear dynamics and determine the DA. In this master's project, the student will carry out online optimization experiments to tune the ring nonlinear lattice and improve the DA and injection efficiency into the storage ring.

List of Figures

1.1 Schematic view of the SIRIUS installations. 1) Linear accelerator (LINAC); 2) Concrete tunnel housing the booster accelerator and the storage ring; 3) storage ring; 4) beamlines. From LNLS website. 17
1.2 Storage ring typycal configuration. From [?] 18
1.3 Schematic representation of the magnets comprising SIRIUS lattice and their fields profile. From left to right: dipole magnet, quadrupole magnet and sextupole magnet. 19
2.1 The Frenet-Serret coordinate system. From [1]. 27
2.2 Betatron functions for the SIRIUS storage ring. Colored blocks represent the magnets of the accelerator lattice: blue for dipoles, orange for quadrupoles and green for sextupoles. The ring has a 5-fold symmetry, with the lattice and betatron function repeating the same pattern shown above five times up to $s = 518$ m 30
2.3 Phase space ellipse traced by tur-by-turn (TbT) motion in the (x, p_x) phase space. Optics functions determine the principal axes ratios and the inclination of the ellipse at each longitudinal position along the ring. From [2]. 31
2.4 Dispersion fucntion for SIRIUS superperiod. 32
2.5 Resonance lines in tune space up to 2nd, 3rd and 4th order, respectively. . 38
5.1 Objective function history vs. iterations of the first trial at beam-loss optimization. 54
5.2 Injection conditions for DA optimization 54
5.3 Objective function vs iterations during the first run of injection efficiency optimization 55
5.4 Objective function vs iterations during the second run of injection efficiency optimization 55
5.5 Current losses vs. horizontal dipole kick for the ref. config. and for the RCDS solutions at WP 1. 57
5.6 Current losses vs. horizontal dipole kick for the initial configuration and the RCDS solutions at WP 2. 57
5.7 Measured phase space at SA05 high-beta straight section for the ref. config. and the best RCDS configurations of runs 1, 2 and 3 in WP 1. Color-map indicates the turns. The areas are in mm mrad. The beam was being kicked horizontally at 730 µrad in the ref. config, 790 µrad in run 1, 780 µrad in run 2, and 770 µrad, in run 3. Loss rates of 12%, 11%, 13% and 13%. . . . 58

5.8 Measured phase space at SA05 high-beta straight section for the initial configuration and the best RCDS configurations of runs 1 and 2 in WP 2. Color-map indicates the turns. The areas are in mm mrad. The beam was being kicked horizontally at 680 µrad, for the initial configuration, 770 µrad for run 1, and at 720 µrad for run 2. Loss rates of 10%, 12% and 12%, respectively 58
5.9 Current losses vs. horizontal dipole kick for the initial configuration and the RCDS solution at WP 3 59
5.10 Measured phase space at SA05 high-beta straight section for the non-optimized configuration and the best RCDS configuration in WP 3. Color-map indicates the turns. The areas are in mm mrad. 59
5.11 Horizontal/Vertical RMS orbit variations in units of the horizontal and vertical beam sizes. Blue curves represents variations in the nominal working point, WP1, orange curves are the orbit variations at WP3, and green curves variations at WP3 plus results of the recent improvements in Fast Orbit Feedback System. From [?] 60

List of Tables

4.1 SIRIUS sextupole families . . . 51
5.1 Chromaticity measurements for ref-config and sextupole configs. found at the second round of injection optimization . . . 56
5.2 Injection efficiencies (IE) for configurations found for Working Points 1, 2 and 3. . . . 59

Contents

1. Introduction **14**
1.1 Storage ring-based synchrotron light sources . . . 14
1.2 The SIRIUS project . . . 16
1.3 Subsystems and components of a storage ring-based light source facility . . 17
1.4 The problem addressed in this work . . . 19

2. Theoretical Background **23**
2.1 The physics of electron storage rings . . . 23
2.2 Motion of charged particles in magnetic fields . . . 25
2.3 The coordinate system for storage ring dynamics . . . 25
2.4 Hamiltonian for the relativistic electron . . . 26
2.5 Specification of magnetic fields . . . 28
2.6 Linear Dynamics . . . 29
2.7 Dispersive & Chromatic Effecs and Linear Perturbations . . . 32
2.8 Nonlinear Dynamics, Perturbations, Ressonances and Tune-Shifts . . . 36

3. Online Optimization **39**
3.1 Defining Online Optimzation . . . 39
3.2 Justifying Online Optimization . . . 40
3.3 Robust Conjugate Direction Search . . . 41
3.3.1 Line methods . . . 41
3.3.2 Powell's conjugate direction set . . . 43

4. Diagnostics tools, measurements processes & experimental setup **46**
4.1 Diagnostics and measurements at the control room . . . 46
4.1.1 Beam Position Monitors . . . 46
4.1.2 Beam Current and Injection Efficiency . . . 47
4.1.3 Tunes measurement & control . . . 47
4.1.4 Chromaticity measurements & control . . . 48
4.2 The choice of objective function . . . 50
4.2.1 Injection scheme for acummulation at SIRIUS storage ring . . . 50
4.3 Selection of optimization knobs . . . 50
4.3.1 Characterization of Sextupole Magnets Configurations . . . 51

5. Experiments and Results **53**
5.0.1 Kick resilience optimization - december 2022 . . . 53
5.0.2 Injection efficiency optimization - december 2022 . . . 54

5.0.3 Optimization experiments throughout 2023 56
5.1 Conclusions 60

6. Discussion and Conclusions **62**

Bibliography **64**

A. Proof of the necessary condition for vectors conjugacy **65**

B. Algorithms Pseudocode **68**

C. Momentum Compaction Factor and the relation between energy deviations and RF frquency changes **71**

Chapter 1

Introduction

This dissertation concerns the work performed on the SIRIUS storage ring sextupole mangets with the objective to optimize the ring's Dynamic Aperture (DA) and injection efficiency. The text is organized as follows:

- The present chapter introduces synchrotron light sources, the SIRIUS project, the main components and subsystems found in electron storage rings and the problem addressed during the execution of the student's masters project;
- Chapter 2 introduces the theoretical and scientific background on the dynamics of particles in accelerators. The optics functions, the tunes, chromatic effects, field errors and perturbations and the dynamic aperture are discussed;
- Chapter 3 introduces and justifies online optimization of nonlinear dynamics in accelerators and presents the Robust Conjugate Direction Search (RCDS) algorithm;
- Chapter 4 describes the experimental methods and setup for the online optmization experiments and the results achieved;
- Chapter 5 concludes this dissertation presenting the final remarks.

1.1 Storage ring-based synchrotron light sources

Synchrotron radiation (SR) is the electromagnetic radiation emitted by charged relativistic particles when accelerated perpendicularly to their motion. The phenomenon was theoretically predicted in the early 1900s when Liénard and Wiechert calculated the retarded potentials for point particles. The first experimental observation occurred at General Electric's synchrotron accelerator, justifying the adoption of the term "synchrotron" in its name [3].

Synchrotron light is extermely colimated and has a broad spectral distribution, covering from infrared to hard X-rays. These properties make synchrotron light ideal for imaging experiments in crystallography and spectroscopy in a wide variaty of scientific disciplines.

Modern synchrotron light sources primarily rely on two particle acceleration technologies: free-electron lasers and electron storage rings. Here, we focus on storage ring-based synchrotron light source facilities. In these facilities, ultra-relativistic electron beams are stored for extended periods within a chamber in ultra-high vacuum to produce synchrotron light. The beams are maintained in stable orbits by the fields of an array of magnets which provide both bending and focusing of the trajectories. The beam is also periodically influenced by radiofrequency cavities, which replenish the energy radiated away in the form of light.

The main figure of merit for the quality of a SR source is the *brightness* [4], defined as the photon flux in six-dimensional phase space [5]:

$$B(\omega) = \frac{1}{\Delta\omega/\omega}\frac{F(\omega)}{\Sigma_x(\omega)\Sigma_y(\omega)}, \tag{1.1}$$

where $F(\omega)$ is the photon flux at energy $E = \hbar\omega$, Σ_u is the photon beam volume in the the $u = x, y$ phase space, and $\Delta\omega/\omega$ is the frquency bandwith, which is typically about 0.1%. The photon phase space volume depends on the convolution of the electron beam distribution with the distribution of the photons emitted by a single electron. The latter depends on the photon energy and the emission process, while the former is related to the average phase space volume of the electron beam: the *emittance*, which depends on the magnetic lattice and has units of the transverse phase space areas (length times angle). Increasing brightness depends on maximizing the photon flux, reducing the electron beam emittances and optimizing the matching between photon and electron beams for maximizing their distributions convolution [3].

Synchrotron light sources can be classified based on their brightness/emittance. In the early 1960s, the community interested in SR for imaging experiments obtained SR parasitically from high-energy and nuclear physics machines such as DESY and DORIS in Germany and ADA in Italy [6], marking the era of first-generation synchrotron light sources [7]. The second-generation machines emerged in the 1980s and consisted on machines designed exclusively for SR production, such as BESSY, DORIS II and III, ELSA in Germany, SUPERACO in France, MAX I in Sweden [6] and UVX in Brazil.

The 1990s saw a growing demand for higher brightness, leading to the development of third-generation machines [7]. These machines introduced insertion devices such as wigglers and undulators, significantly enhancing brightness by increasing radiative damping. Additionally, these devices allowed precise control over radiation energy and polarization. Typical emittances for third-generation machines is of the order of units to tens of nm rad. Most of currently operating machines pertain to the third-generation, such as ALBA in Spain, ESRF and SOLEIL in France, Diamond in the United Kindom and ELETTRA, in Italy [6].

The era of the fourth-generation of storage rings (4GSR) commenced with the commissioning of the MAX-IV machine in Lund, Sweden, in 2015 [5, 7]. Fourth-generation machines achieved a notable reduction in emittance, reaching sub-nm rad values thanks to recent technological advancements in computer simulations, vaccum technology, machining and mechanical alignment [5, 7]. Following MAX-IV, an upgrade of the ESRF facility, the ESRF-EBS, and the launch of SIRIUS in Campinas marked significant milestones for the fourth-generation. Today, several 4GSR projects are being planned, designed and constructed.

1.2 The SIRIUS project

SIRIUS is a 4GSR synchrotron light source. It was designed, built, and is operated by the Brazilian Synchrotron Light Laboratory (LNLS), on the campus of the Center of Research in Energy and Materials (CNPEM), in Campinas, Brazil. The storage ring operating energy is 3 GeV, and the ring has 518 m in circumference. The natural emittance of the lattice is 250 pm rad and it is expected to reach 150 pm rad with the installation of its definitive insertion devices [8][1].

SIRIUS succeeded the first synchrotron light source in Brazil, the UVX machine, which opened to users in 1997 and served the community until its shutdown, in the beginning of SIRIUS commissioning, in August 2019[2] [8]. The project started in 2009, initially planned and designed as a third-generation machine. By 2012, it evolved into the project of a fourth-generation machine [8]. Cunstruction was finished in 2018, the LINAC and Booster commissioning soon followed. In november 2019 the first beam was stored in the storage ring.

Check these statemets. Get more info about main milestones

SIRIUS finished its Phase-0 commissioning in 2022 and since March 2023 is receiving its first external users. At the time of this writing, it has 6 operating beamlines, 4 beamlines in commissioning and 4 under construction and installation. It is currently storing 100 mA current, with frequent beam injections throughout the day, a scheme known as “top-up” mode. SIRIUS is expected to achieve 350 mA current when the system of two superconducting radiofrequency cavities is installed [9, 10].

more info on the phases. which phase are we in?

Presently, SIRIUS stands as the most complex scientific infrastructure ever consturcted in Brazil, with the ambitious goal of positioning the country at the forefront of global leadership in synchrotron light sources. This state-of-the-art synchrotron was

[1]SIRIUS is currently operating with provisional insertion devices for providing light to the first users and allowing scientific commissioning of the beamlines

[2]The UVX project led to the creation of LNLS, which marked a new model for scientific research in Brazil, based on social organizations under contracts with the Ministry of Science Technology and Innovations. LNLS paved the way for national labs (NL), including labs on biosciences (LNBio), nanotechnology (LNNano), and bio-renewables (LNBR), which are also located at the CNPEM campus.

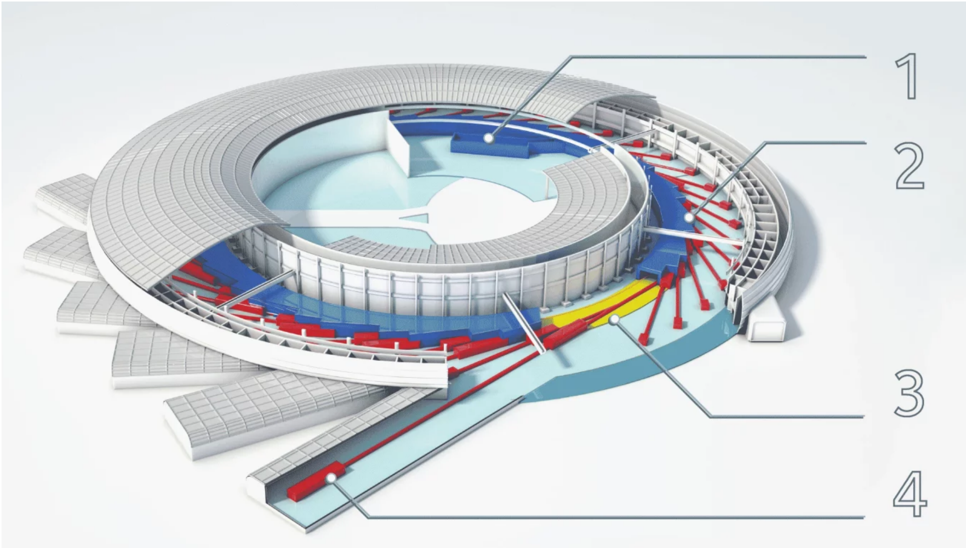

Figure 1.1: Schematic view of the SIRIUS installations. 1) Linear accelerator (LINAC); 2) Concrete tunnel housing the booster accelerator and the storage ring; 3) storage ring; 4) beamlines. From LNLS website.

meticulously designed to shine as the brightest in its energy category, and has the capacity to host up to 40 beamlines. As of the time of this writing, SIRIUS holds the distinction of being the sole fourth-generation synchrotron light source in the southern hemisphere and one of merely three 4GSRs in operation across the globe (still true?).

1.3 Subsystems and components of a storage ring-based light source facility

Typical systems comprising a storage ring synchrotron light source facility include:

- an injection system: including the electrons source, beam transport lines, the linear accelerator and the booster circular accelerator. At SIRIUS, the linear accelerator provides the booster ring with a 150 MeV beam. The booster further ramps the beam energy up to 3 GeV, which is the storage ring operation energy;
- storage ring: where the ultra-relativistic beam of electrons is kept in stable orbits for hours within the vaccum-chamber, producing synchrotron light at the bending magnets and insertion devices;
- beamlines which steer the photon beams towards the experimental cabins where samples are placed for the experiments based on light-matter interaction, such as spectroscopy, crystallography, tomography and others.

A schematic view of the SIRIUS building is shown in Fig. 1.1.

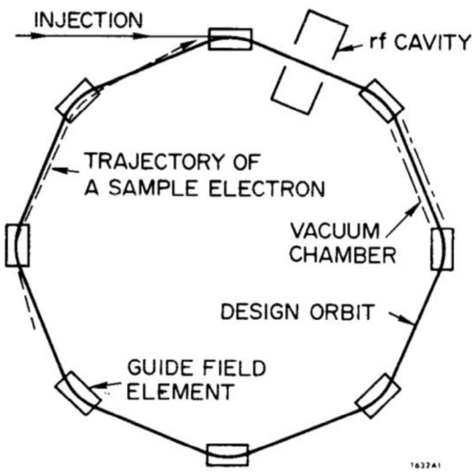

Figure 1.2: Storage ring typycal configuration. From [?]

Storage ring magnets and RF cavity

draw my onw figure

Figure 1.2 sketches the typical layout of a syncrhotron accelerator. The electron beam is stored within a vaccum chamber, oscillatin in proximity to a reference design closed orbit under the influence of an array of magnets. The orbit is determined by the strengths of the deflection magnets, the dipoles, and the operation energy of the beams. A pure dipole magnet provides an uniform and homogeneous magnetic field perpendicular to the facility floor and bends the electrons trajectory in the direction parallel to the floor. For the trajctories resulting in a closed orbit, the overall bending angle provided by the dipoles along the entire ring must equal 2π radians. The field profile of a dipole magnet is depicted in the left side sketch of Fig. 1.3. Imagining a beam directed inward the screen, the trajectory will be bent to the right.

To maintain electrons in close proximity to the reference orbit, focusing of the trajectories is required. Focusing is attained by employing gradient fields, primarily generated by quadrupole magnets at SIRIUS. The strength of such fields increase linearly with deviations from the closed orbit, which lies in the magnet's center. Gradient fields effectively act as spring forces. The mangets poles and the field profile of a quadrupole magnet are depicted in the center sketch of Fig. 1.3.

Focusing and deflection are energy-dependent, which means small deviations from the nominal operating energy can result in differential focusing. Drawing an analogy from geometric optics, the beam's focusing behavior at the "lens" (quadrupoles) depends on its "color" (energy). To correct for these chromatic aberrations, the use of "glasses" becomes necessary. In the context of accelerators, sextupole fields serve as these corrective lenses. They introduce geometric aberrations to counteract the chromatic ones, resulting in approximately uniform, energy-independent focusing, up to the linear approximation theory. The mangets poles and the field profile of a sextupole magnet are depicted in the right sketch of Fig. 1.3.

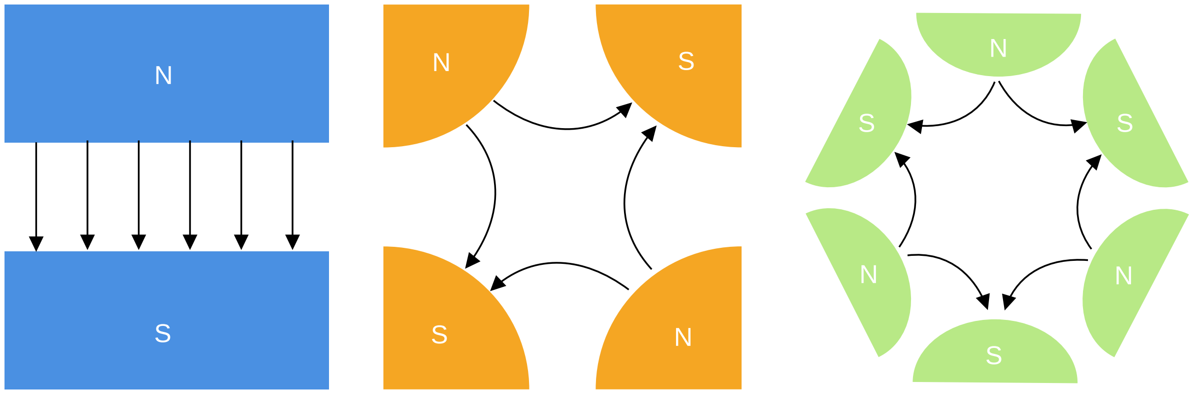

Figure 1.3: Schematic representation of the magnets comprising SIRIUS lattice and their fields profile. From left to right: dipole magnet, quadrupole magnet and sextupole magnet.

Besides dipoles, quadrupoles and sextupoles, additional dipole actuators magnets for orbit/trajectory correction and pulsed magnets for beam injection are also part of the ring. The beam is also periodically subject to longitudinal time-dependent electromagnetic radiofrequency fields which do work on the beam to replenish its energy. The goal is to compensate for the energy carried away in the form of synchrotron light.

1.4 The problem addressed in this work

The pursuit of low emittances and high brightness has driven the accelerator community toward the fourth-generation of storage rings. Achieving such low emittances was possible because of series of technological advances which enabled the use of the multi-bend achromat (MBA) lattice [5, 7]. MBA lattices require intense gradient fields provided by quadrupole magnets, which, in turn, demands the presence of strong sextupolar fields to compensate for chromatic effects. Since sextupoles provide nonlinear fields, the dynamics in fourth-generation storage rings has become increasingly nonlinear [7].

A quasi-periodic nonlinear dynamics, when subjected to even the slightest perturbations—such as small field errors stemming from rotation, alignment, or fields excitation errors—can potentially become unstable at large oscillation amplitudes. These instabilities impose constraints on the maximum transverse oscillation amplitudes that the machine can accommodate. The specific amplitude below which motion is stable is referred to as the Dynamic Aperture (DA) of the ring. Exceeding the DA results in irregular and often chaotic motion and beam loss.

Under normal operating conditions, the equilibrium beam size and typical oscillation amplitudes are considerably smaller than the DA, and the dynamics can be well studied and analyzed using a linear approximation theory, without worrying about the DA. However, there are specific scenarios where the DA becomes crucial for the operation, notably during the injection process.

During injection into the storage ring for beam accumulation, the beam is extracted from the booster accelerator and guided toward the storage ring through a transport line. As soon as it enters the ring, the beam is deflected by the field of a pulsed nonlinear magnet, which makes the beam almost parallel to the storage ring tangent direction, albeit with a horizontal offset of approximately $x = -8$ mm [11]. If the DA is smaller than this initial amplitude, it imposes limitations on the injection efficiency.

The placement, symmetry and strength of sextupoles magnets–the nonlinear lattice– were determined through a multi-objective optimization process, primarily focused on improving the simulated DA and beam lifetime of the machine's computer model [12,13]. This optimization work considered the average performance of the lattice configurations while accounting for various magnet errors that simulate the expected errors in the actual machine [12]. Several models, with several errors distribution among the magnets were generated, and the DA and lifetime for a given lattice configuration was calculated by simulating the electron beams motion for several turns (tracking simulations). The final figure of merit for a lattice consisted on the average DA and lifetime it provided to the ensemble of machines. The best-performing machine lattice found during this process was adopted as the nominal lattice which was subsequently deployed during the commissioning phase of the machine.

The operating machine consists on a practical realization of a specific error configuration, which defines the physically realized magnetic lattice and determines the dynamics overall performance. The best-performing lattice on average, found in the simulations, is not necessarily the optimum lattice for this specific errors realization.

Assuming the realized lattice closely approximates the optimum setup, i.e. that the errors are small, it is reasonable to assume that by making minor tweaks and adjustments to the strengths of the sextupoles one can adapt the nonlinear lattice to match the actual distribution of errors in the physical system. This fine-tuning process can result in improved nonlinear dynamics performance, expanding the DA, and ultimately enhancing both injection efficiency and its stability. This process has already been demostraded in other machines. It has proven to be a succesfull approach and became knonw as *Online optimization*. If one thinks of the errors as agents that deteriorate the DA from its optimum, online optimization can be seen as an attempt to compensate for such deterioration.

Online optimization of the machine nonlinear dynamics consists on employing computer-automated search strategies to systematically explore various sextupole configurations with the goal of identifying the ones that yields the largest DA while not interfering in other machine parameters, such as chromaticity and beam lifetime. The key ingredient in online optimization is the choice of a robust optmization algorithm based on direct or indirect search in the parameter space. The most widely used is the Robust Conjugate Direction Search (RCDS) algorithm, which is based on a noise robust one-dimensional optimizer along with a clever strategy, known as Powell's method, for choosing directions in the search space. Chapter 3 addresses the RCDS algorithm.

Besides improving the DA and injection efficiency in nominal operation conditions, it is also interesting to do so in different machine *working points*, with different *tunes*. As chapter 2 shows, if one fixes one's attention to a specific point of the ring, and measure the beam position in horizontal and vertical planes for consecutive turns, one realizes the motion is a sampled sinusoid and the tunes ν_x and ν_y are the fundamental frequencies of such harmonic motion. They are important operation parameters since they affect over the response of the system in the presence of pertrubations. Tunes close to integer numbers result in large *orbit amplification factors* making the dynamics particularly sensitive to perturbations.

The fractional parts of SIRIUS nominal tunes are quite low and increasing them would distance the tunes away from integer numbers, reducing the orbit amplification factors and improving the orbit stability. Changing the tunes can be achieved by actuating with the quadrupole magnets, but doing so takes the machine to a different operating optics, in which the DA can, and often is, smaller than the DA in nominal optics. In different working points, thus, online optimization is essential to find a new sextupole configuration to adapt the nonlinear mangets to the new optics and achieve a good DA and acceptable injection efficiencies for operation.

In agreement with the experience in other facilities, it is shown in Chapter 4 that online optimization using RCDS can succesfully improve the dynamics performance and lead to DA and injection efficiency improvements. This was observed for the SIRIUS storage ring both in the machine nominal tunes as well as in other working points. SIRIUS experience with online optimzation is a valuable demonstration of this tool's efficiency in fourth-generation rings with such a large search space.

At the time of this writing, SIRIUS is operating with the sextupole configurations found during one of the experiments carried out during the execution of this project. The configuration was found by online optimzination carried out with increased tunes optics. The higher tunes led a reduction in obrit amplification factors resulting in unprecedent orbit stability.

In the next chapter, the dynamics of electrons in storage rings is examined. The linear approximation motion is introduced and nonlinear dynamics is trated as a perturbation to the linear theory. Chapter 3 gives the reader a brief overview of optimization strategies and focuses on familiarizing the reader with the Robust Conjugate Direction Search (RCDS) algorithm. Chapter 4 presents the methods and results of the online optimization experiments carried during the execution of this project.

Chapter 2

Theoretical Background

This chapter provides the bare minimum theoretical knowledge on electron storage ring physics and particles dynamics needed to state to the reader the optimization problem and the constraints which are involved. A qualitative description of the physics of electron storage rings is presented, followed by a more detailed and more quantitative treatment of single particle dynamics in storage rings.

2.1 The physics of electron storage rings

As mentioned previously, a storage ring is designed to confine bunches of electrons and steer them along a reference closed orbit. The orbit is defined by the bending magnets, the dipoles. The trajectories consist on oscillations about the closed orbit, and focusing of such oscillations toward the closed orbit is provided by gradient fields, mostly coming from quadrupole magnets. Additionally, to correct chromatic aberrations in the beam's motion, i.e. a dependence of focusing with the beam's energy, and guarantee correct focusing despite energy deviations from the nominal value, sextupolar magnetic fields are also introduced, providing fields depending qudratically on the deviations from the nominal orbit. These fields introduce strong nonlinearities in the dynamics.

When having its trajectory bent at the dipoles and insertion devices, the beam loses energy in the form of synchrotron radiation. To mantain the beam stored, the energy lost must be replenished. To this aim, radio-frequency (RF) cavities are placed along the ring to provide oscilating electric fields parallel to the longitudinal direction. The work done in the beam by the fields restore its energy.

The radiated photons are emitted in a narrow cone with angular aperture of $1/\gamma$, γ being the relativistic Lorentz factor (~ 6000 at SIRIUS storage ring). The photons carry away a fraction of the beam's energy and momentum in both the longitudinal and transverse directions. When passing through RF cavities, only momentum in the longitudinal direction is replenished. The combined effect of radiating photons and passing throgh RF cavities leads to an overall damping of transverse amplitudes.

On the other hand, the quantum nature of the emitted radiation leads to the excitation of transverse oscillations, which is known as quantum excitation. When a photon carries away energy, it depletes the electrons energy by the same amount. It thus changes the reference orbit of the electron in certain regions of the ring (dispersive regions), inducing oscillations. Eventually, equillibrium between radiative damping and quantum excitation is achieved, leading the rms values of each electron's amplitudes to reach a stationary regime.

include the case of nondispersive and vertical amplitudes damping

Each one of the beam's degrees of freedom defines an acceptance: limits which if exceeded can result in instabilities and eventually beam losses. The most obvious acceptance is the transverse acceptance: the beam motion is bounded by a vacuum chamber and colliding with the chamber's physical apperture leads to losses. Additionally, the beam also has an energy acceptance: a tolerance for energy deviations from the nominal value that when exceeded can lead to a suboptimal energetic balance, which, in turn, leads to significant deviations from the nominal orbit and eventually collisions with the vacuum chamber.

The beam is also subject to elastic and inelastic collisions with residual gas molecules within the chamber and also the collisions between electrons within the same bunch, besides other kinds of interactions with wake-fields from other bunches. All these effects can lead to beam-losses and the overall beam loss rate resulting from these combined mechanisms defines the characteristic time scale at which a given electron current survives in the ring. This is the beam lifetime and determines the rate at which injections into the storage ring are required.

Because of the nonlinearities introduced by the sextupole magnets, the transverse acceptances can be limited not solely by the physical aperture available in the vaccum chamber but rather by the amplitudes above which motion is irregular, unstable and unbounded. As already mentioned before, this limiting amplitude is known as the dynamic aperture (DA), a term that can be used to refer to amplitudes in the transverse space x, y or to the phase space coordinates x, p_x and y, p_y.

Despite the complicated physics of a fully-coupled dynamics involving the transverse and the energy oscillations and also the damping and the excitation of amplitudes, collective effects and instabilities, for the purpose of this dissertation, it is sufficient to model the motion of a single electron, negletcting radiation losses (and thus the existence of the RF cavities) and any other collective interactions.

In this picture, the electron travels along the ring at the speed of light and executes transverse oscillations in two orthogonal planes. The dynamics takes place in a 4-dimensional phase space which is the dynamics of two independent quasi-periodic oscillators. These simplfications are justified for our immediate purposes because:

- radiation losses/gains and energy oscillations are only significant over a time scale of a couple of turns. Over this period, tens of transverse oscilations take place

- the linear and uncoupled dynamics this modeling renders serves as a building block upon which ellaborate modeling can be carried out, incoporating coupling, nonlinearities and perturbations with perturbation theory
- why is it ok to ignore collective effects and instabilities?

Next, the single-particle dynamics is presented with the aim of defining quantitavely the dynamic aperture and the characteristics of the dynamics in electron strorage rings. Throghout the modelling, optical functions and parameter for the SIRIUS storage rings are also presented.

2.2 Motion of charged particles in magnetic fields

An electron of charge e and momentum of magnitude p follows a circular orbit of radius ρ when interacting with an uniform and time-independent magnetic field of magnitude B directed perpendicularly to the ortbit plane. In such conditions, the Lorentz force law predicts that the relevant quantities are related by

$$R(p) \equiv B\rho = \frac{p}{e}. \tag{2.1}$$

Consider now an electron traveling along a curve parametrized by the arclength s with respect to an arbitrary reference point. The interaction with fields $B_x(x, y, s)$ and $B_y(x, y, s)$, both perpendicular to the electron's motion, results in deflections of the trajectory. The deflection angles are given by

$$\mathrm{d}\theta_u = \frac{\mathrm{d}s}{\rho_u(s)} = \frac{e}{p}B_v(x, y, s)\mathrm{d}s = \frac{1}{R(p)}B_v(x, y, s)\mathrm{d}s, \quad u, v = x, y \quad \text{or} \quad y, x. \tag{2.2}$$

Where (2.1) has been used to replace the p/e ratio by the *magnetic rigity* $R(p)$, which is defined as the product of the uniform field strength needed for a beam with momentum p and charge e to perform circular orbit with radius ρ. The rigidity depends solely on the electron's momentum/energy and gives the appropriate normalization to evaluate the instantaneous angular deflections in the electron's trajectory caused by magnetic fields.

Add deflection figures

2.3 The coordinate system for storage ring dynamics

As sketched by Figure 1.2, electrons in a storage ring perform a prescribed nearly circular trajectory close to a reference orbit. A convenient coordinate frame to decribe the dynamics in storge rings can be constructed by imagining a reference particle traveling along a curve drawn by the tip of a vector $\mathbf{r}_0$, as Fig. 2.1 shows. The idea is that this particle samples exactly the reference nominal orbit. The particle travels a distance s along the ring, which can be used to parametrize the motion. The triad of direction vectors consists of a vector $\hat{\mathbf{s}}$, tangent to the trajectory, a vector $\hat{\mathbf{x}}$ normal to it, pointing in the direction at which $\hat{\mathbf{s}}$ changes and a vector $\hat{\mathbf{y}} = \hat{\mathbf{x}} \times \hat{\mathbf{s}}$, bi-normal to the trajectory. This construction leads to a Frenet-Serret reference frame. The deviations from the nominal orbit can be measured in units of the unit vectors in the normal and bi-normal directions, characterizing the transverse dynamics. One may also be concerned with the distance of a given particle from the reference particle itself along the curce. Such differences may arise due to differences in the energy two particles. Since no radiation loss nor gain will be considered in our modeling, the energy and longitudinal deviations from the reference particle are not dynamical quantities, but rather parameters of the dynamics.

Assuming no curvature in the y plane, i.e. that the accelerator defines a curve whose plane is parallel to the facility flat floor, then the unit vectors defining the frame can be calculated by [14]

$$\hat{\mathbf{s}} = \frac{\mathrm{d}\mathbf{r}_0}{\mathrm{d}s}, \quad \hat{\mathbf{x}} = -\rho \frac{\mathrm{d}\hat{\mathbf{s}}}{\mathrm{d}s}, \quad \hat{\mathbf{y}} = \hat{\mathbf{x}} \times \hat{\mathbf{s}}. \tag{2.3}$$

where $\rho(s) = \|\mathrm{d}\hat{\mathbf{s}}/\mathrm{d}s\|^{-1}$ is the local curvature radius[1]. The vectors evolve along s as prescribed by the Frenet-Serret equations:

$$\frac{\mathrm{d}\hat{\mathbf{s}}}{\mathrm{d}s} = -\frac{1}{\rho(s)}\hat{\mathbf{x}}, \quad \frac{\mathrm{d}\hat{\mathbf{x}}}{\mathrm{d}s} = \frac{1}{\rho(s)}\hat{\mathbf{s}}, \quad \frac{\mathrm{d}\hat{\mathbf{y}}}{\mathrm{d}s} = 0, \tag{2.4}$$

The frame thus depends solely on the geometry of the specified path. Since the curvature is defined by the dipolar fields $B_0(s)$ in the y direction, then, eq. (2.2) leads to

$$\frac{1}{\rho(s)} = \frac{B_0(s)}{R_0}, \tag{2.5}$$

where R_0 is the rigidity for the beam at the nominal energy.

2.4 Hamiltonian for the relativistic electron

The dynamics of relativistic electrons influenced by electromagnetic fields $(\Phi, \mathbf{A})$ is encapsulated by the Hamiltonian [15]

$$H = \sqrt{m^2c^4 + (\mathbf{P} - q\mathbf{A})^2c^2} + e\Phi,$$

[1] For a circular trajectory, $\mathbf{r}_0 = (R\cos(s/R), R\sin(s/R), 0)$, $0 \leq s \leq L$ (check), in the cartesian laboratory frame. $\hat{\mathbf{s}} = (-\sin(s/R), \cos(s/R), 0)$, $\mathrm{d}\hat{\mathbf{s}}/\mathrm{d}s = -R^{-1}(\cos(s/R), \sin(s/R), 0)$ and $\rho(s) = R$, justifying the interpretation as curvature radius.

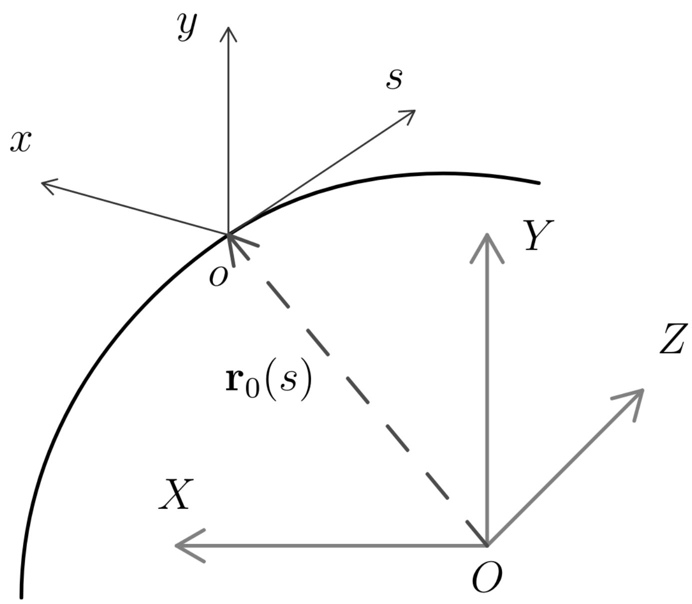

Figure 2.1: The Frenet-Serret coordinate system. From [1].

e being the elementary charge and $\mathbf{P} = \mathbf{p} + e\mathbf{A}$ the canonical momentum. The following steps are followed to obtain equations of motion for electrons in the storage ring:

- A canonical transformation to change coordinates is applied in order to describe the motion in terms of the Frenet-Serret frame variables x, y;
- Instead of time t, the Hamiltonian and the dynamical variables are described as functions of s, the longitudinal position along the ring;
- Paraxial approximation: the transverse momenta are assumed to be way smaller than the momentum along the trahectory's tangent direction. This allows the expansion of the the square root in the Hamiltonian as a power series, revealing the expression for an approximate Hamiltonian which can be more easily handled;
- Geometric quantities are used: in the paraxial approximation, the canonical momenta for on-energy particles are identified with the derivatives with respect to the parameter s $x' = \mathrm{d}x/\mathrm{d}s$ and $y' = \mathrm{d}y/\mathrm{d}s$, which represent the divergence angles from the nominal orbit;

All of the transformations and manipulations summarized above can be found in detail in the litereature, such as in Refs. [2,3,14]. As mentioned previously, by neglecting RF cavities ($\Phi = 0$) and radiation losses, the energy will a constant parameter and the dynamics will consist solely on the transverse degrees of freedom. In this 4-dimensional dynamics, the set of canonical variables are (x, p_x, y, p_y), where the momenta are given by

$$p_x = x'(1+\delta), \quad p_y = y'(1+\delta) \tag{2.6}$$

and δ is the relative deviation from the nominal energy-momentum:

$$\delta \equiv \frac{P - P_0}{P_0} \approx \frac{E - E_0}{E_0}. \tag{2.7}$$

The ultra-relativistic approximation $E \approx pc$ was used.

Hamilton's equations for the paraxial-approximated Hamiltonian reveals the equations of motion for the x and y Frenet-Serret coordinates, which read:

$$x'' = -\frac{(1+Gx)^2}{1+\delta}\frac{B_y}{R_0} + G(1+Gx), \quad y'' = \frac{(1+Gx)^2}{1+\delta}\frac{B_x}{R_0}, \tag{2.8}$$

where $R_0 = p_0/e$ is the magnetic rigidity of the beam at the nominal energy and $G(s) \equiv \rho^{-1}(s)$ is the inverse local radius of curvature, related to the dipole field as in Eq. (2.5).

2.5 Specification of magnetic fields

To study the motion, we need to specify the fields $B_x(s)$ and $B_y(s)$ acting on the beam. Since in a storage ring the magnets are arranged as arrays of dipoles, quadrupoles and sextupoles which usually have some symmetry and periodicity, the $B_x(s)$ and $B_y(s)$ functions are generally periodic. If $\ell_\mathrm{d}, \ell_\mathrm{s}, \ell_\mathrm{s}$ are the lengths of dipoles, quadrupoles and sextupoles magnets in a ring, respectively, the magnetic fields are sectionally defined and have the following functional forms

- Horizontal Dipole

$$B_x(s) = 0, \quad B_y(s) = B_0, \quad s \in (0, \ell_\mathrm{d}), \tag{2.9}$$

- Normal quadrupole

$$B_x = B_1 y, \quad B_y = B_1 x, \quad s \in (0, \ell_\mathrm{q}), \tag{2.10}$$

- Normal sextupole

$$B_x = B_2 xy, \quad B_y = \frac{1}{2}B_2(x^2 - y^2), \quad s \in (0, \ell_\mathrm{s}), \tag{2.11}$$

and zero everywhere else, neglecting the fields of insertion devices. Fields (2.9)–(2.11) are the so-called *normal multipole fields*. There are also *skew multipole fields*, which couple the horizontal and vertical dynamics. We will neglect skew fields and coupling for now. They can be treated as perturbations in perturbation theory schemes.

In eqs. (2.8), the magnetic rigidity normalizes all the fields. We therefore define the normalized dipolar, quadrupolar and sextupolar fields as the functions

$$G(s) = \frac{B_0(s)}{R_0}, \quad K(s) = \frac{B_1(s)}{R_0}, \quad S(s) = \frac{B_2(s)}{R_0}. \tag{2.12}$$

add plot of the S, K and S functions

2.6 Linear Dynamics

The linear equations of motion

Expansion of eqs. (2.8) up to first order in the x, y, δ variables leads to [16]

$$x'' + (G^2 + K)x = G\delta, \quad y'' - Ky = 0. \tag{2.13}$$

For on-momentum particles, $\delta = 0$, both equations are instances of Hill's equations

$$u'' + K_u(s)u = 0, \tag{2.14}$$

i.e, a pair of parametric oscillators for $u = x, y$, with s-dependent and periodic focusing functions

$$K_x(s) = G^2(s) + K(s), \quad K_y(s) = -K(s),$$

the analogues to an oscillator's spring force per unit mass. Motion in the linear approximation thus consists on oscilations around the closed orbit, known as *betatron oscillations*.

Pseudoharmonic description

Betatron motion can be cast in a amplitude-phase form. One can show that

$$u(s) = \sqrt{2\beta_u(s)J_u}\cos(\phi_u(s) + \phi_0), \quad u = x, y, \tag{2.15}$$

is a solution to (2.14) as long as the $\beta_u(s)$ function satifies the boundary-value problem

$$\frac{1}{2}\beta_u'' + \beta_u K_u(s) - \frac{1}{\beta_u}\left(\frac{1}{4}\beta_u'^2 + 1\right) = 0, \quad \begin{cases} \beta_u(0) = \beta_u(L) \\ \beta_u'(0) = \beta_u'(L) \end{cases} \tag{2.16}$$

and the phase advance is given by

$$\phi_u(s) = \int_0^s \frac{1}{\beta_u(\sigma)} \mathrm{d}\sigma. \tag{2.17}$$

The motion is oscillatory, non-harmonic and non-periodic. The oscillations envelope is the square-root of the beta functions $\beta_u(s)$, which for the SIRIUS storage ring are shown in Fig. 2.2.

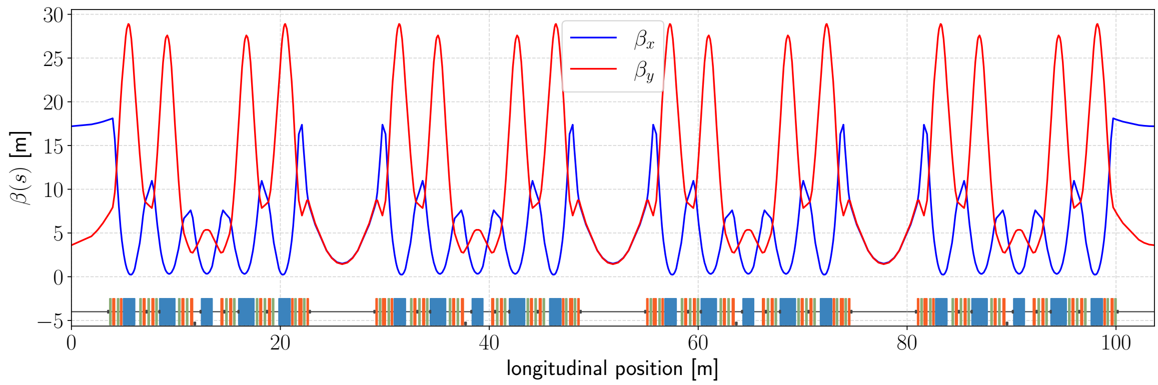

Figure 2.2: Betatron functions for the SIRIUS storage ring. Colored blocks represent the magnets of the accelerator lattice: blue for dipoles, orange for quadrupoles and green for sextupoles. The ring has a 5-fold symmetry, with the lattice and betatron function repeating the same pattern shown above five times up to $s = 518$ m

The tune

An important feature of the dynamics is the *tune*: the phase advance over a revolution along the ring

$$\nu_u = \frac{1}{2\pi} \int_s^{s+L} \frac{\mathrm{d}\sigma}{\beta_u(\sigma)} \equiv \frac{1}{2\pi} \oint \frac{\mathrm{d}s}{\beta_u(s)}.$$

The tune reveals the number of transverse oscillations per revolution. The nominual tunes for SIRIUS storage ring are $(\nu_x, \nu_y) = (49.08, 14.14)$.

When studying the effects of perturbations and nonlinearities acting on the beam, one finds the tunes are a critical variables in determining the beam's response. More specifically, the tunes impact over disturbances amplifiction factors, which are greatest when tunes are close to integer numbers.

Turn-by-turn motion

If one keeps track of the time evolution of the the u, u' variables at a fixed position along the ring, plotting them in a phase space, one realizes the the quasi-periodic motion traces out ellipses in such plane. This fact can be analytically verified by calculating the derivative

$$u'(s) = -\sqrt{\frac{2J_u}{\beta_u}}\left[\sin(\phi_u(s)+\phi_0) + \frac{1}{2}\beta_u'(s)\cos(\phi_u(s)+\phi_0)\right], \tag{2.18}$$

defining the functions $\alpha_u = \frac{\beta_u'}{2}$ and $\gamma_u = \frac{(1+\alpha_u^2)}{\beta_u}$ and checking that u, u' satisfy the quadratic form

$$2J_u = \gamma_u u^2 + 2\alpha_u u u' + \beta_u u'^2. \tag{2.19}$$

The ellipse properties are ruled by the $\beta_u(s), \alpha_u(s)$ and $\gamma_u(s)$ functions, also known as Courant-Snyder (C-S) parameters or Twiss parameters. Since the parameters are functions of the position s, then, at each point along the accelerator, the Poincaré Section u, u' displays a different ellipse. Although different in shape, their areas are proportional to J_u, an invariant quantity determined by the particle's initial condition. The areas are thus conserved along the ring [3, 14].

Since the phase advance over a turn is $2\pi\nu + \phi_0$, the phase advance after the j-th turn is $2\pi\nu j + \phi_0$, and thus sampling the transverse motion at a fixed $s = s_0$ position reveals a harmonic displacement, which at the j-th turn reads

$$u_j(s_0) = \sqrt{2\beta_u(s_0)J_u}\cos(2\pi\nu_u j + \phi_u(s_0)). \tag{2.20}$$

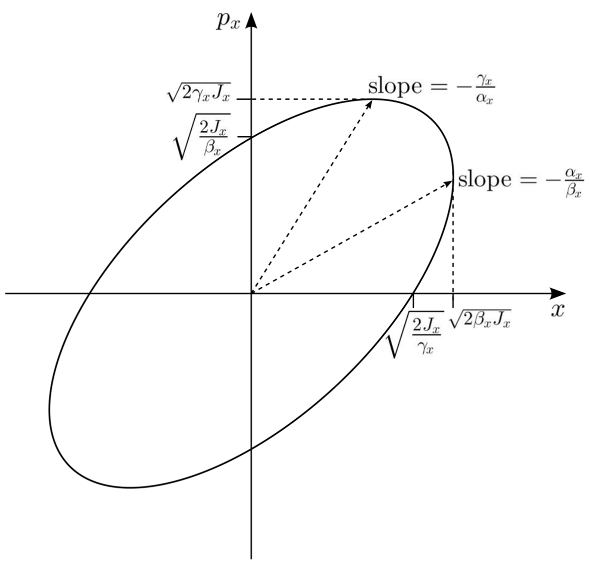

Figure 2.3: Phase space ellipse traced by tur-by-turn (TbT) motion in the (x, p_x) phase space. Optics functions determine the principal axes ratios and the inclination of the ellipse at each longitudinal position along the ring. From [2].

2.7 Dispersive & Chromatic Effecs and Linear Perturbations

Dispersion

The equation of motion for off-momentum particles in the horizontal plane, the first of eqs. (2.13), is a non-homogeneous Hill's equation. The solution consists on the linear combination of the homogeneous solution (betatron motion) plus the particular solution: $x = x_\beta + x_\delta$. Since the non-homogeneous term, $G(s)\delta$, is proportional to δ, we can assume $x_\delta = \eta(s)\delta$ where $\eta(s)$ is the *dispersion function*, which should satisfy

$$\eta'' + (G^2 + K)\eta = G, \qquad \begin{cases} \eta(0) = \eta(L), \\ \eta'(0) = \eta'(L). \end{cases}$$

The periodicity in the $\eta(s)$ function is required if we want to interpret it as a closed orbit distortion per relative momentum deviation. Thus, off-momentum particles perform betatron oscillations around a dispersive orbit, displaced from the nominal orbit by $\eta(s)\delta$. The dispersion function for the SIRIUS storage ring is shown in Fig. 2.4

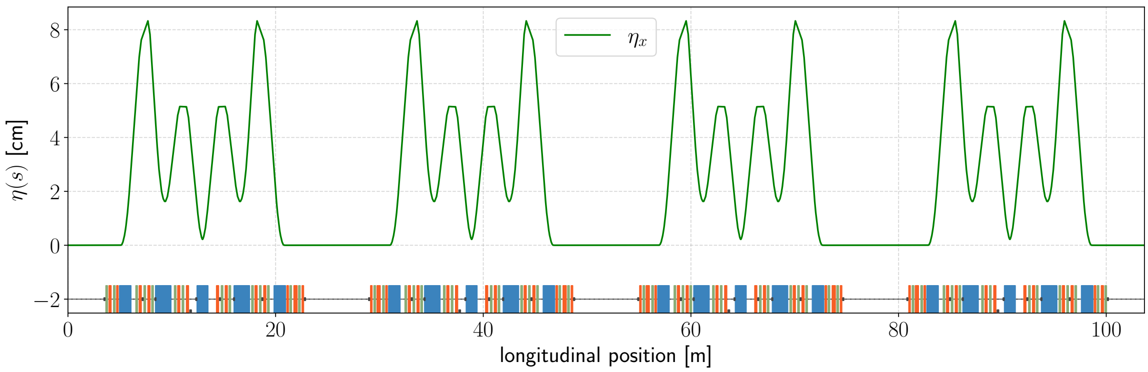

Figure 2.4: Dispersion fucntion for SIRIUS superperiod.

Linear Field Errors

In the presence of additional dipolar and quadrupolar fields representing field errors and deviations from the nominal fields, the orbit and focusing of the beam are changed. Assuming these are small perturbations and not sufficiently strong to kill the beam, we can evaluate the disturbances to the unperturbed dynamics. The details and derivations can be found in the literature, such as in chapter 2 of Ref. [14]. Here we highlight the main results.

For dipole errors $\Delta G_y(s) = -\Delta B_{0x}(s)/R_0$ and $\Delta G_x(s) = \Delta B_{0y}(s)/R_0$, the equations of motion read

$$x'' + K_x(s)x = G\delta + \Delta G_x(s), \quad y'' + K_y(s)y = \Delta G_y(s). \tag{2.21}$$

The solution consists on the combinations of the betatron motion plus the dispersive orbit (for the horizontal plane) plus the closed orbit distortion u_{co} induced by the additional bending terms due to the dipole errors. For a single thin bending error ΔG_u in the $u = x, y$ plane, acting for a length Δs around $s = s_0$, the closed orbit distortion u_{co} reads

$$u_{\mathrm{co}}(s) = \frac{\sqrt{\beta_u(s)\beta_u(s_0)}}{2\sin\pi\nu_u}\Delta G_u \cos(\pi\nu_u - |\phi_u(s) - \phi_u(s_0)|)\Delta s. \tag{2.22}$$

For a distribution $\Delta G_u(s)$ of dipolar perturbations along the ring, we sum over the contributions:

$$u_{\mathrm{co}}(s) = \frac{\sqrt{\beta_u(s)}}{2\sin\pi\nu_u}\int_s^{s+L} \Delta G_u(\sigma)\sqrt{\beta_u(\sigma)}\cos(\pi\nu_u + \phi_u(s) - \phi_u(\sigma))\,\mathrm{d}\sigma\,. \tag{2.23}$$

The prefactor involving the sine of the tune shows how ν_u close to an integer can amplify the effects of the dipolar perturbations on orbit distortions. At first sight, aiming for tunes half-integer tunes $\nu = k/2, k \in \mathbb{Z}$ might seem desireable to minimize the distortions. Choosing so, however, increases the sensitivity to gradient errors, which we examine next.

Gradient errors can be modeled as corrections to the focusing functions in the equations of motion: $K_u(s) \to K_u(s) + \Delta K_u(s)$, for $\Delta K_x(s) = \Delta B_{1y}(s)/R_0$ and $\Delta K_y(s) = -\Delta B_{1x}(s)/R_0$. The changes in beam focusing lead to changes in the beta-functions, phase advances and consequently the betatron tunes. One can show the tune-shift as a consequence of a gradient error acting over a small extent Δs around $s = s_0$ is [14]

$$\Delta\nu_u = \frac{1}{4\pi}\beta(s_0)\Delta K_u \Delta s. \tag{2.24}$$

For a distribution of errors we sum over the ring:

$$\Delta\nu = \frac{1}{4\pi}\oint \beta(s)\Delta K(s)\mathrm{d}s, \tag{2.25}$$

where the closed integration sign refers to a complete circulation along the ring, i.e., integration from s_0 to $s_0 + L$, for any $s_0 \in [0, L)$.

As for the induced error on the beta-functions, it is possible to show that the relative error, known as betabeat, can be expressed as

$$\frac{\Delta\beta_u(s)}{\beta_u(s)} = -\frac{1}{2\sin(2\pi\nu_u)}\int_s^{s+L} \Delta K_u(\sigma)\cos[2(\phi_u(\sigma) - \phi_u(s) - \pi\nu)]\mathrm{d}\sigma. \tag{2.26}$$

which is the largest for $2\nu_u$ closest to an integer. This means we must avoid tunes close to half-integers if we want to avoid the coherent build-up of betatron amplitudes, which can eventually lead to beam loss. Integer or half-integer tunes are the simplest instances of resonances the beam can be subject to. A more general overview of resonances is presented in section 2.8.

Chromaticity

We know the bending angles at the dipoles is different for electrons with different energies. This is the origin of dispersive orbits. The energy deviations affect not only the closed orbit by means of the dispersion effect, but affect also the focusing of the trajectories, since a more/less energetic beam has higer/lower rigidity and thus is focused differently when passing through gradient fields. Expanding the equations of motion, eqs. (2.8), for off-energy particles up to the order of terms $u\delta$, for $u = x, y$, reveals additional higher-order gradient errors. The focusing functions are corrected by $K_u(s) \to K_u(s) + \Delta K_u(s)$ [1, 14], where

$$\Delta K_x = -(K + 2G^2)\delta \approx -K_x\delta \tag{2.27}$$

$$\Delta K_y = K\delta = -K_y\delta \tag{2.28}$$

This means there exists an energy-dependent tune-shift effect caused by the gradient error. Using eq. (2.25), the tune-shift reads

$$\Delta\nu_u = -\frac{1}{4\pi}\oint \beta_u K_u \delta \, \mathrm{d}s\,, \tag{2.29}$$

for the $u = x, y$ planes. We can define the *linear chromaticity* in the $u = x, y$ direction as tune-shift $\Delta\nu_u$ per relative energy deviation δ:

$$\xi_u = \frac{\mathrm{d}\nu_u}{\mathrm{d}\delta}. \tag{2.30}$$

This uncorrected chromaticity is also called natural chromaticity. Using expression (2.29) for the tune-shift, the natural chromaticity reads

$$\xi_{u,\text{nat}} = -\frac{1}{4\pi}\oint K_u\beta_u \, \mathrm{d}s\,. \tag{2.31}$$

This chromatic aberration effect needs to be corrected to guarantee energy-independent focusing. Correction can be attained with the insertion of geometric aberrations provided by sextupolar fields, specifically in the dispersive sections of the storage ring. In such regions, off-energy particles follow a dispersive orbit, and their position reads $x(s) = x_\beta(s) + \eta(s)\delta$, where $x_\beta(s)$ consists on the betatron oscillations. Since sextupolar fields are of the form

$$B_x = B_2 xy, \quad B_y = \frac{B_2}{2}(x^2 - y^2),$$

then, the off-momentum particles "see" the fields

$$B_x = B_2(x_\beta y + \eta\delta y), \quad B_y = \frac{B_2}{2}(x_\beta^2 - y^2) + B_2 x_\beta \eta\delta + \frac{B_2}{2}(\eta\delta)^2,$$

So, to lowest order in eqs. (2.8), they feel a dipolar perturbation (which contributes to orbit distortions) and the gradient perturbation

$$\Delta K_{x,y}(\delta) = \pm S\eta\delta,$$

recalling that $S(s) = B_2/R_0$.

Considering the contributions from both the errors induced by energy deviations and also the lowest order sextupole gradient effect, we have a total error of $\Delta K_u = -(K_u \mp S\eta)\delta$ to be inserted in eq. (2.25). The chromaticity in a lattice with sextupoles thus reads

$$\xi_u = -\frac{1}{4\pi} \oint \beta_u (K_u \mp S\eta)\, \mathrm{d}s\,, \tag{2.32}$$

with the minus sign for $u = x$ and the plus sign for $u = y$. The chromaticity depends linearly on sextupole strengths, allowing for its correction to desired values. Since the effect of the sextupole field focuses in a given plane but defocuses in the other, at leas two sextupole families are requiered for chromaticity correction: one familiy where $\beta_x > \beta_y$ and other where $\beta_y < \beta_x$. The cost of correcting chromaticity is the insertion of perturbations and nonlinearities in the dynamics. To allow for more control over the nonlinear dynamics effects, usually some families of sextupoles are also placed in non-dispersive sections. They are called acrhomatic families, since they have no effect over chromaticity.

Missing figure

show chromatic aberrations and their correction with geometric aberrations

2.8 Nonlinear Dynamics, Perturbations, Ressonances and Tune-Shifts

Action-Angle Variables

The betatron equations of motion, Eqs. (2.14), can be obtained as Hamilton's equations for an effective, linear Hamiltonian

$$\mathcal{H}_u = \frac{1}{2}u'^2 + \frac{1}{2}K_u(s)u^2, \tag{2.33}$$

summed over $u = x, y$. A transformation $(u, u') \to (\psi_u, J_u)$ to Action-angle variables is implicitly implemented by the type–1 generating function [14]

$$F_1(u, \phi_u) = \int u'\, \mathrm{d}u = -\frac{u^2}{2\beta_u}\left(\tan\phi_u - \frac{\beta_u'}{2}\right). \tag{2.34}$$

The action variable reads

$$J_u = -\frac{\partial F_1}{\partial \phi_u} = \frac{u^2}{2\beta_u}\sec^2\phi_u = \frac{1}{2\beta_u}[u^2 + (\beta_u u' + \alpha_u u^2)], \tag{2.35}$$

from which we can recover the pseudo-harmonic form $u = \sqrt{2\beta_u J_u}\cos(\phi_u(s) + \phi_0)$. In the J, ϕ variables, the new hamiltonian is $H_0(\phi, J)$, given by

$$H_u = \mathcal{H}_u + \frac{\partial F_1}{\partial s} = \frac{J_u}{\beta_u}. \tag{2.36}$$

Performing the change to action-angle variable in both the horizontal and vertical planes we find the action-angle Hamiltonian for 4D dynamics

$$H_0 = \frac{J_x}{\beta_x} + \frac{J_y}{\beta_y}. \tag{2.37}$$

Hamilton's equations read

$$\phi_u' = \frac{1}{\beta_u(s)}, \qquad J_u' = 0. \tag{2.38}$$

Perturbations and tune-shifts

Linear motion is integrable, since it can be written in terms of the action variable only (angle-independent Hamiltonian). This leads to the action variable being a constant of motion, and the phase advance behaving just as the pseudo-harmonic motion anticipated.

Linear motion, though, is only a useful first approximation. In reality, in an storage ring, there are higher order multipole magnets, such as sextupole magnets, and also multipole, alignement and excitation errors, all acting as perturbations to linear motion. Generically referring to perturbations as $V(J,\phi)$, we can write the perturbed motion Hamiltonian

$$H(J,\phi) = H_0 + V(J,\phi), \tag{2.39}$$

For which Hamilton's equations read

$$\phi'_u = \frac{1}{\beta_u(s)} + \frac{\partial V(J,\phi)}{\partial J_u}, \quad J'_u = \frac{\partial V(J,\phi)}{\partial \phi_u}. \tag{2.40}$$

The action is no longer an invariant and the phase advance rate deviates from the linear betatron phase advance.

Phase space ellipses distortions and phase accumulation deviations

Focusing on the effects on the tunes, we can be express the tunes in terms of the nonlinear chromatic and amplitude-dependent tune-shifts

$$\nu_u = \nu_{u0} + \xi_u(\delta)\delta + \alpha_{uu}J_u + \alpha_{uv}J_v \tag{2.41}$$

where ξ_u represents the energy-dependent tune-shifts (higher order generalization of the linear chromaticity), and the other components consist on the amplitude-dependent tune-shifts, up to first order in the actions.

Ressonances

4D linear and unperturbed motion consists on the motion of two uncoupled parametric oscillators. As a quasi-periodic, integrable system, the phase-space is diffeomorphic to the 2-Torus, $\mathbb{T}^2$, and there are an infinite number of such tori covering phase space, corresponding to the different choices of initial conditions J_u.

Canonical perturbation theory applied to perturbed motion fails to converge whenever the ratio of tunes is sufficiently rational. The Poincare-Birkhoff theorem states that under such conditions, almost all the periodic phase-space orbits disappear. An even number of tori survives, half of which are stable and half unstable. Unstable motion in a storage ring can eventually lead to beam loss.

The condition for sufficiently rational tunes can be expressed as

$$m\nu_x + n\nu_y = \ell, \tag{2.42}$$

for $n, m, \ell \in \mathbb{Z}$. This condition defines lines in tune-space corresponding to the locus in which perturbation theory fails and motion can become unstable. These are resonance lines and $|n| + |m|$ is the order of the resonance. Particular ressonances arising from linear field errors, such as dipolar errors, $\nu_x, \nu_y = n \in \mathbb{Z}$, and gradient field errors, $2\nu_x, 2nu_y = n \in \mathbb{Z}$, are contained in condition (2.42). Resonances coupling both planes arise when considering perturbations the skew multipole magnets, which can be treated by perturbation theory. Linear coupling resonances are the famous sum and difference resonances $\nu_x + \nu_y = \ell, \nu_x - \nu_y = \ell$, excited by skew quadrupoles magnets.

more detials, and the resonances induced by sextupoles

Figure 2.5 shows resonance lines for the resonances up to second, third and fourth order respectively. First order resonances can be excited by dipolar fields, 2nd order resonances can be excited by quadrupole fields and 3rd order resonances can be driven by sextupolar fields.

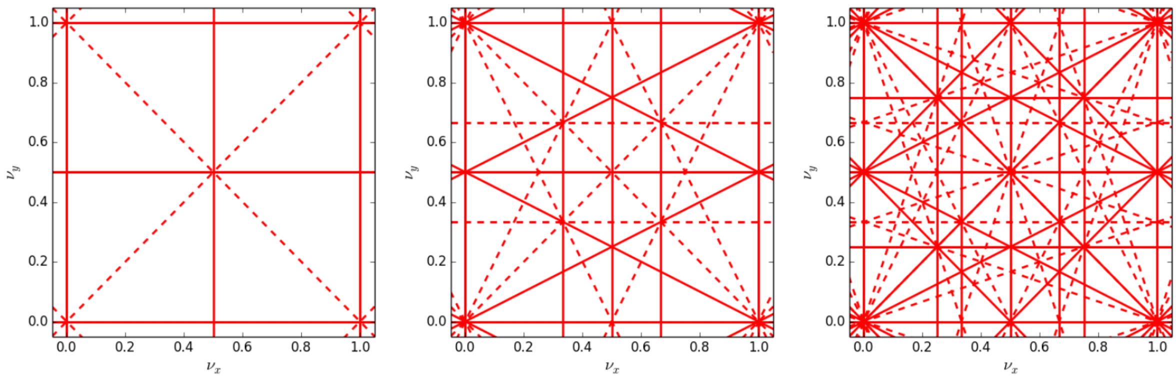

Figure 2.5: Resonance lines in tune space up to 2nd, 3rd and 4th order, respectively.

Dynamic Aperture

Nonlinear dynamics can become sensitive to initial conditions when the amplitudes are large. Because of the tune-shfits, specially the amplitude-dependent tune shifts, the tunes can wander in tune space, eventually crossing resonance conditions that may lead to instabilities, chatotic motion and beam loss. The dynamics can impose limitations to the maximum transverse deviations in which the beam can oscillate while displaying regular and bounded motion. This is a dynamic restriction to the motion known as the *dynamic aperture*.

Exceeding the dynamic aperture eventually leads to beam loss. During injection of the beam, if the transverse offsets are larger than the dynamic aperture, the beam is not captured into the storage ring. This is specially important for off-axis injection, such as in the case for SIRIUS.

More discussion on DA.

Chapter 3

Online Optimization

This chapter defines, introduces and justifies online optimization in the context of accelerators. A bief overview of optimzation algorithms and their classifications is presented. The Robust Conjugate Direction Search (RCDS) algorithm is introduced as well as the other rountines from which it was derived from.

This chapter adds no novelty to the literature in optimization. It is just an overview for merely pedagogic purposes. It is mostly based on the disscussion presented by the classic Numerical Recipes, as well as Refs.

3.1 Defining Online Optimzation

Suppose we have a machine (we do) in which there is some sort of figure of merit depending on the collective state of some set of relevent components, parts or operation modes–our parameters. There is no mechanistic/deterministic or probabilistic model for the dependence of the figure of merit on the reparameters state, but we do know the parameters affect the figure of merit. We may call these relevant parameters as knobs, since we can use them to tune the figure of merit.,

Now suppose we want to tune the knobs so the figure of merit reches a certain value, or so that it is minimized or maximized. This is an optimization problem, and we might as well call the figure of merit our objective function. Since the whole system is a black-box, to measure diferent values for the objective function, i.e., to sample it, we need to change the knobs and measure it again. The tuning procedure is thus based on trial-and-error.

If we are able to devise a computer-automated strategy to seek for the desired value or extremum of the objective function, then running this program while the machine is up and working is what we define as online optimization. The program must measure the objective function and read the current state of the knobs, calculate/decide and apply the changes on the knobs, measure the objective again and evaluate and judge the quality of the changes carried out. The process is iterated until the desired outcome is reached.

This black-box, heuristic optimzation problem describes the Dynamic Aperture otpimzation problem very well. The DA is a figure of merit related to the nonlinear dynamics–in SIRIUS' case, the sextupole magnets. There is no analytical/statistical[1] model prediciting DA changes given sextupole nudges so we cannot invert the problem and tune sextupoles to A desired DA value. The tuning procedure must be based on trial-and-error.

3.2 Justifying Online Optimization

Running online optimization in a machine will find the nearest extremum (minimium/maximum). In other words, if no stochacity element is brought into the routine to diversify the search along the parameter space, it will find local, not global extrema. How can we be sure the local minima are the best solution for the optimization problem?

It seems that we will never know, but it actually does not matter. A good-performing solution is all we care about as long as other operation parameters are not affected (more details on the next chapter). But there are reasons to believe the local minima found are actually the global ones and it has to do with how accelerators are designed and the origins of deterioration of the dynamic aperture in the machine.

Because there are correction schemes for the linear dynamics in accelerators, the Dynamic Aperture, i.e. limitations to the allowed oscillation amplitudes, arises because of perturbations acting in a nonlinear dynamics. Other than that, the only limitation would be the physical aperture[2]. The strength and symmetry of the whole magnets lattice is decided based on simulating several possibile machine lattice configurations and evaluating parameters such as the dynamic aperture and the beam-lifetime. The best performing and viable solution (lattice) is implemented in the real machine.

In the real machine, additional errors arising from magnets misalignment or any fields deviations can (and will) introduce additional perturbations and can deteriorate the DA. The simulating procedure actually does take into consideration the existence of errors: they are introduced in the model during evaluation of the figure of merit parameters and the best performing lattice on average is chosen.

In the machine, a particular error configuration is physically realized, and we are thus dealing with one possible lattice realization, for which the optimum configuration is not that with the largest average DA or lifetime. But we expect it to be not too far from that reference configuration chosen and applied to the machine. Online optimzaiton thus consists on adjusting the sextupole lattice to the physically realized machine lattice so that it reaches its best-performing configuration.

[1] in principle, a surrogate model could be trained to reproduce dynamic aperture given the sextupole strengths as inputs. This is not what we have done so far

[2] Unperturbed nonlinear motion can display no limitations to oscillation amplitudes

3.3 Robust Conjugate Direction Search

Optimization routines and algorithms are usually classified according to whether they rely on the calculation of derivatives (gradient-based) or solely on the comparison of the objective function values (gradient-free). The latter can yet be classified into direct- or indirect-search methods, depending on whether the search of the extremum relies on direct comparisons of the objective function itself or from a mathematical model of it, respectively [?].

Both gradient-based and gradient-free strategies rely on the comparison of the objective function at different points of the parameter space. If the objective function suffers from noise this can significantly reduce the efficiency of the optimization routine [?,?]. In Chap. 7 of Ref. [?], a review of the most popular optimization algorithms shows how most of them suffer to find minima to, at least, the precision of the noise-σ the objective function is subjected to.

The Robust Conjugate Direction Search (RCDS) algorithm is a indirect-search, gradient-free optimization algorithm introduced in Ref. [?]. The algorithm consists of a main loop for constructing and managing optimal search directions along the knobs space (Powell's Method) and a one-dimensional optimizer responsible for a noise-aware search for the minimum along a given direction. The algorithm is capable of optimizing the objective function (find its local maximum/minimum) to at least the precision of the objective-function noise [?, ?], being thus adequate for online optimization problems. Specifically, for accelerator controls and optimization, the algorithm has been successfully applied to optimize beam steering and optics matching during injection [?], reducing horizontal emittance [?, ?]and optimization of dynamic aperture [?, ?, ?, ?, ?].

RCDS actually consists on small modifications of well-known indirect-search routines. To grasp how it works, a brief overview on its predecessors is presented next.

3.3.1 Line methods

Let us incorporate the role of an accelerator operator and suppose we are seeking the configuration of a single knob rendering the best peformance, say, the minimum of a certain figure of merit. We nudge the knobs slowly and measure the objective, scanning for the minimum. We might scan tuning the knobs up while the objective goes downhill, and stop when starts increasing. The knobs lives over the real line, so this is basicaly a line-scan, the basis of line optimization methods. How to teach a computer do the same?

Let $f(x) \in \mathbb{R}$ be the objective function depending on the single parameter $x \in \mathbb{R}$. The task of optimizing f is achieved by a direct search over its domain. Since maximizing a function equals to minimizing the same function multipled by -1, in what follows, we shall refer to minimization only.

The search for the minimum is usually preceeded by initially *bracketing* the miminum. We seek for points $a < b < c$ in the domain such that $f(b)$ is smaller than both $f(a)$ and $f(c)$. If f is reasonably smooth, we are certain there will be a minimium in the interval (a, c). Standard bracket routines for well-behaved, noiseless objective functions can be found in the literature, and mostly consists on, starting from an initial point, scanning the line “downhill" until the function stops decreasing.

We can see the bracketing procedure as a coarse-grained scan initially performed by the operator. The minimum is then finely searched on a second line-search scan. Given an intial bracketed interval, the most common line-search methods are

- Golden Section Search: which progressively scans within the brackets, updating it at each iteration so that it shrinks at each round until it spans only a small interval specified by the user. The machine precision ϵ is often indicated. The guess for the miminum is taken as the mid-point along the interval. The minimum point is found to within the precision of $\epsilon/2$.

- Parabolic Interpolation: where a parabola is fitted to the values $f(a), f(b), f(c)$ the function takes along the brackets. Moving along the parabola minimum takes us to f's minumum or pretty close to a it in a single leap.

The brackets routine and the line-search methods presented rely on the comparison of the objective function at different points in the parameter space. They assume the functions to be deterministic and trust the behaviour and are completely unaware of the experimental noise.

In what follows, we assume what we actually measure in the control-room is $\hat{f}(x) = f(x) + \xi$, where $\xi \sim \mathcal{N}(\mu = 0, \sigma)$ is a random variable modeling the experimental noise, with σ being expected noise error, $\sigma^2 = \mathrm{Var}[\xi]$.

For the optmization of noisy objective functions, RCDS introduces a noise-aware bracketing routine and a parabolic interpolation scan over the bracket interval. For the brackets, instead of seeking for points $a < b < c$ satisfying $f(b) < f(a), f(b) < f(c)$, RCDS requires a more strict condition $f(b) < f(a) + 3\sigma, f(b) < f(c) + 3\sigma$. This increase the likelihood the observed trend consists on real trends of the objection itself, rather than random errors.

During the line-search, a parabola is fitted within the brackets and its minimum is taken as the objective function minimum. Additionally there is a comparison of the available (previously evaluated) points within the brackets used for the fitting of the parabola. If any of them is considered an outlier, it is discarded and the fitting is repeated without it.

Missing figure

bracketing and linescan illustrations

3.3.2 Powell's conjugate direction set

How could we optimize an objective function $f(\mathbf{x}) \in \mathbb{R}$ depending on the set of p parameters $\{x_i\}_{i=1,\ldots,p}$? The simplest idea is to iteratively optimize nudging each knob individually: optimize f by changing x_1, while the other knobs remain fixed. Next, optimize by changing x_2 only, and so forth. In other words, each one of the knobs defines a direction whose basis vector is $\hat{\mathbf{e}}_i$, correspoinding to a unit change of the knob. This is easy to automate with the noise-robust line-optimzer introduced in the previous section.

Formally, we are reducing a multi-dimensional optimzation problem into a series of line-searches. That is, given an intial configuration of the parameters (an initial position) $\mathbf{x}_0$, and a direction $\hat{\mathbf{n}}$, we have the one-dimensional problem to minimize $g(\delta) = f(\mathbf{x}_0 + \delta\hat{\mathbf{n}})$. The minimum is then $f(\mathbf{x}_0 + \delta_*\hat{\mathbf{n}})$, where $\delta_* = \arg\min_\delta g(\delta)$. In the previous paragraph, we specialized to $\mathbf{n} = \hat{\mathbf{e}}_i$, and iterated for $i = 1, \ldots, p$.

Missing figure

basis vectors minimization vs conjugate directions

As can be seen in figure, scanning along each orthogonal directioon can be time-consuming, specially for some functions with long narrow valleys at some angle with the coordinates basis vectors. This strategy thus is suboptimial when evaluation of the objective function is expensive.

The reason why using unit basis vectors can be so inneficient is because optimizing along a given basis vector spoils down minimization carried out in the any other of them. So the processes needs to be iterated. A more efficient strategy consists on constructing a set of special non-interfering direction vectors for which the minimizationsare preserved when optimizing in a different driection.

The necessary condition for direction vectors $\mathbf{u}$ and $\mathbf{v}$ to be non-interfering is (proof in the apendix)

$$\mathbf{v} \cdot \mathbf{H} \cdot \mathbf{u} = 0, \tag{3.1}$$

where $(\mathbf{H})_{ij} = \partial^2 f(\mathbf{x}_0)/\partial x_i \partial x_j$ is the Hessian matrix for function f. The $\mathbf{u}$ and $\mathbf{v}$ directions are said to be conjugate directions.

The problem now consists on finding an appropriate set of p conjugate directions, so we can optimize $f(\mathbf{x})$ along them. Let $\{\mathbf{u}_i\}$ denote our directions set. Powell proved conjugate directions can be constructed as follows

1. Set the initial directions as the basis vectors: $\hat{\mathbf{u}}_i = \hat{\mathbf{e}}_i, i = 1, \ldots, p$.
2. Save the starting point (initial parameters state) as $\mathbf{x}_0$;
3. For $i = 1, \ldots, p$ minimize along $\hat{\mathbf{u}}_i$. Save the minimimum as $\mathbf{x}_i$.
4. For $i = 1, \ldots p - 1$ set $\hat{\mathbf{u}}_i \leftarrow \hat{\mathbf{u}}_{i+1}$
5. Set $\mathbf{u}_p = \mathbf{x}_p - \mathbf{x}_0$. Normalize to obtain $\hat{\mathbf{u}}_p$.
6. Minimize along $\hat{\mathbf{u}}_p$. Name the found minimum as the new $\mathbf{x}_0$ and repeat the procedure until reaching a certain number of evaluations or until some stopping condition is reached.

That is, from steps 1–3. we optimize along each one of the unit basis vectors, updating the minimum. When finishing optimization along x_p, the current minimum will be $\mathbf{x}_p$. In step 4 we discard the first direction, rename directions $\mathbf{u}_{i+1}$ to $\mathbf{u}_i$, and set as our new pth direction the vector from the starting point $\mathbf{x}_0$ to the the current minimum.

Powell proved that repeating this procedure k times for a quadratic form produces a set of directions whose last k vectors are mutually, pairwise conjugate, in the sense of the Hessian matrix. So p iterations exactly minmizes the quadratic form. The method is also quadratically convergent: each iteration doubles the number of significant figures of the candidate minimum for the quadratic form.

There is a problem in throwing away for $\hat{\mathbf{u}}_1$ for $\mathbf{x}_p - \mathbf{x}_0$ every iteration: at some point the lines start to fold up on each other and lose linear independence. As a result the function can end up minimized only within a subspace of parameter space. To fix this, you can reinitialize the directions to the basis vectors after an iteration along the p directions, or use any new set of orthogonal directions.

The somewhat counterintuitive solution suggested by Powell is to discard not necessarily $\hat{\mathbf{u}}_1$ in favor of the new direction, but the direction along which f had its largest decrease so far. This is justified because this direction is likely have a largest component along the new proposed conjugate direction. Accepting this advice results in a set of p directions which are no longer mutually conjugate by the end of p iterations. As a result, the method will no longer be quadratically convergent

Powell also posits some conditions in which is best not to add any new directions, keeping the old set from the previous iteration. These are presented in the appendix, as well as the pseudo-code for the Powell loop.

In summary, Powell's direction set loop calculates and manages directions adaptatively, deciding when to change old directions in favor of newly calculated conjugated vectors, and when to avoid the changes to control build-up of linear depencence

In practice, using conjugate directions accounts to finding a good set of directions in which the number of steps along the vectors is reduced. They provide "shortcuts" towards the minimum in the objective landscape.

Chapter 4

Diagnostics tools, measurements processes & experimental setup

This is a "methods" chapter. Its first section presents the available beam diagnostics at the storage ring and describes the experimental measurements of relevant quantities such as beam positions, trajectories and orbits, beam current and lifetime, the tunes and chromaticity and how these are dialed at our will during a study. The last two sections discuss the choice of objective functions to probe the Dynamic Aperture and the appropriate selection of sextupole families as the optimzation knobs.

4.1 Diagnostics and measurements at the control room

4.1.1 Beam Position Monitors

To probe the beam's position along the ring, a diagnostic tool consisting on a set of four pick-up antennas placed within the vaccum chamber are used. These are known as Beam-position-monitors (BPMs), and are sketched in the Figure. The antennas are placed in such a manner so the electron beam deposits mirror charges when passing by then and triggers the antenna a certain voltage signal. The determination of the beam displacements is based on the differential signal induced on the antennas when the beam is not at the geometric center, in which case the induced charges are equal. The signal of the antennas is processed in the so-called "Delta/Sigma" scheme, which gives the horizontal and vertical beam displacements according to the following algebra:

$$x = K_x \frac{(A+D)-(B+C)}{\Sigma}, \quad y = K_y \frac{(A+B)-(C+D)}{\Sigma}, \tag{4.1}$$

where A, B, C, D refers to the intensity of the induced signal over the corresponding antenna, $\Sigma = A+B+C+D$ is the sum signal, proportional to the beam's current, and K_x and K_y are calibration factors, which depend on the BPM geometry and distances between the antennas. SIRIUS has 160 BPMs distributed along the storage ring. They allow for the determination of the centroid's positions at a turn-by-turn acquisition rate, which is needed for probing of the betatron motion. The signal can also be processes in other acquisition rates, which renders an averaging of the singal and allows to probe information about the orbit.

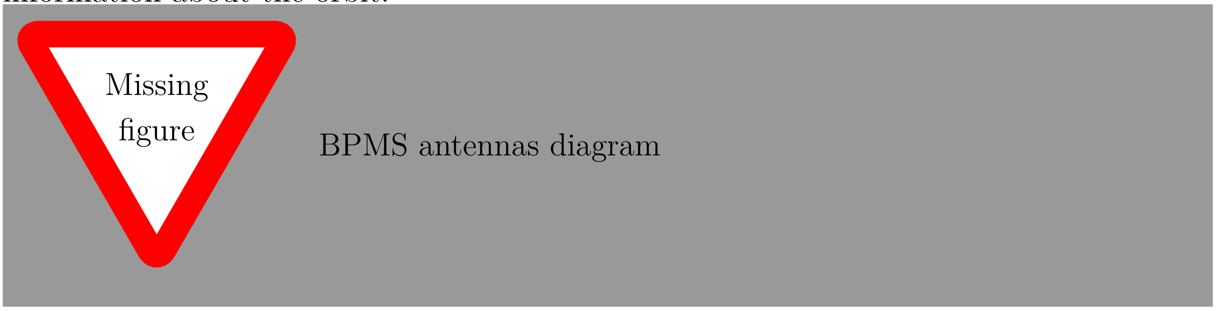

4.1.2 Beam Current and Injection Efficiency

Direct-Current Current Transformers (DCCTs) enable the measurement of the stored beam current within accelerator rings (booster or storage ring). A DCCT current monitor works by surrounding the the beam of charged particles in the accelerator ring with a magnetic core. The magnetic field induced by the beam current flowing by the core is then measured, allowing for an accurate determination of the current itself.

Utilizing the current measurement and the beam revolution period in the respective ring, one can assess the stored charge, and calculate the injection efficiency during storage ring injections. By estimating the charge in the booster or transport line just before injection into the storage ring and the storage ring charge immediately after the injection pulse, is possible to deduce the efficiency of the injection process.The efficiency of the injection can also be estimated from the sum-signal of the BPMs, since it is proportional to the stored current.

what is the accuracy and prcision of the current measurements with the DCCT? what are its limitations? what about the sum-signal

4.1.3 Tunes measurement & control

When turn-by-turn motion is viewed at a fixed longitudinal position s, it consits on the sampling of a harmonic motion. Its fundamental frequency is the tune ν. Any observation of Turn-by-turn (TbT) motion can reveal the tunes upon the appropriate singal processing. For instance, the betatron motion can be Fourier-transformed (discrete Fourier transform via fast-fourier transform algorithm), revealing the BPM signal spectrum. Alternatively the time-domain singal can be fitted to a sinusoid, allowing the determination of the tune as the fundamental frequency.

Precise measurement and online monitoring of the tunes in an accelerator ring can be achieved with the aid of a stripline shaker, which constantly drives the beam with an alternating electric field in a narrow of frquencies, leading to sub-nanometer displacements and inducing small-amplitude, noninterfering with operation betatron motion. The same system also reads back the beam response at that same frequency range. The peak of the beam response signal is identified with the betatron tune.

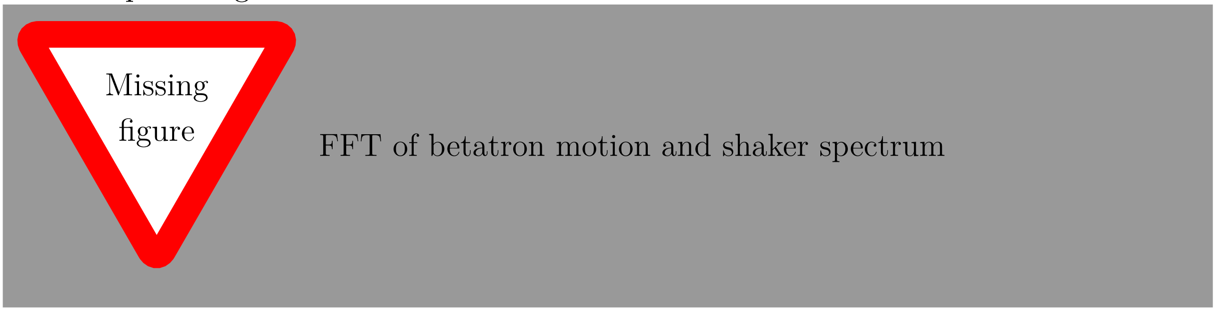

As for changing and manipulating the tunes, formula (2.24) reveals that changes in the quadrupoles strengths, specially at the quadrupoles at large β-function sections, allow for the control of the tunes. Since the tune response to quadrupole strength changes is linear, a tune-response matrix can be constructed, i.e. the Jacobian of the tunes with respect to changes in quadrupoles, so that tune changes can be expressed as

$$\Delta\boldsymbol{\nu} = \mathbf{J}_\nu \Delta\mathbf{K}, \tag{4.2}$$

where $\Delta\boldsymbol{\nu} = \begin{bmatrix}\Delta\nu_x & \Delta\nu_y\end{bmatrix}^\intercal$ is the tune-shifts vector, $\Delta\mathbf{K}$ is the vector containing the changes in stregths across all the quadrupole families, and the Jacobian or response matrix has entries

$$(\mathbf{J}_{\boldsymbol{\nu}})_{ij} = \frac{\partial \nu_i}{\partial K_j} \approx \frac{\Delta\nu_i}{\Delta K_j}, \quad i = x, y, \quad j \in \text{quadrupole families}. \tag{4.3}$$

The system can pseudo-inverted, allowing for the determination of quadrupoles changes required for a desired tune change

$$\Delta\mathbf{K} = \mathbf{J}_\nu^+ \Delta\boldsymbol{\nu} \tag{4.4}$$

where $\mathbf{J}_\nu^+ = (\mathbf{J}_\nu^\intercal \mathbf{J}_\nu)^{-1}\mathbf{J}_\nu^\intercal$ is the Moore-Penrose pseudoinverse.

which families are used when changing tunes? add discussion on chaging the optics when changing tunes

4.1.4 Chromaticity measurements & control

Chromaticity characterizes the energy-dependent tune-shift. To measure it, we need to calculate the numerical derivative

$$\xi_u = \frac{\partial \nu_u}{\partial \delta} \approx \frac{\Delta\nu_u}{\delta}$$

The *momentum compaction factor* establishes the relation between energy deviation induced orbit length changes. Since the revolution period and thus the revolution frequency depend on the orbit length and since the RF frequency is adjusted to match a harmonic of the revolution frequency, a relation can be established between the energy deviations and RF frequency changes

$$\delta = -\frac{1}{\alpha}\frac{\Delta f}{f} \tag{4.5}$$

thus the chromaticity can be measured by instead calculating the numerical derivative

$$\xi_u = -\frac{f}{\alpha}\frac{\Delta \nu_u}{\Delta f} \tag{4.6}$$

Just as the tunes depend on the quadrupoles strengths linearly, chromaticity depends linearly on the sextupole strengths, as eq. (2.32) shows. Chromaticity can be dialed to certain desired values according to the same pseudo-inversion procedure described above for the tunes. We relate the chromaticity changes $\Delta\boldsymbol{\xi} \in \mathbb{R}^2$ to sextupole familiy strength changes $\Delta\mathbf{S} \in \mathbb{R}^{d_s}$ by

$$\Delta\boldsymbol{\xi} = \mathbf{J}_{\boldsymbol{\xi}}\Delta\mathbf{S}, \tag{4.7}$$

where $\Delta\boldsymbol{\xi} = \begin{bmatrix}\Delta\xi_x & \Delta\xi_y\end{bmatrix}^\intercal$ and the Jacobian matrix $\mathbf{J} \in \mathbb{R}^{2\times d_s}$ has entries

$$(\mathbf{J}_{\boldsymbol{\xi}})_{ij} = \frac{\partial \xi_i}{\partial S_j} \approx \frac{\Delta \xi_i}{\Delta S_j}, \quad i = x, y, \quad j \in \text{sextupole families.} \tag{4.8}$$

d_s refers to cardinality of the set of sextupole families used in the chromaticity change process. In principle, at least two families are required for correcting/tuning chromaticity in the machine: one family for each plane. Since the chromatic sextupole families are the only ones effectively changing chromaticity to leading order, then, at most, $d_s = 15$.

If we wish to change chromaticity by a $\Delta\boldsymbol{\xi}$ amount, the jacobian can be pseudo-inverted to calculate the required sextupole strength changes

$$\Delta\mathbf{S} = \mathbf{J}_{\xi}^{+}\Delta\boldsymbol{\xi}. \tag{4.9}$$

In practice the chromaticity jacobian was never actually measured in the real machine, due to the time-consuming process of varying a single sextupole family, carrying out the chromaticity measurement and repeating the processs for the 15 chromatic families. The "measurement" is instead done in the SIRIUS storage ring computer model, since the model-calculated jacobian allows for satisfactory correction or tuning of the chromaticity in the actual machine.

which families are used for correctiing

4.2 The choice of objective function

There is no analytical formula for relating the storage ring linear or nonlinear optics to the Dynamic Aperture. The optimization procedure must be a direct search procedure: changes are performed in the knobs and the effect over dynamic aperture is evaluated.

Also, we cannot measure dynamic aperture directly. We must choose an objective function to act as a probe to the DA: a figure of merit related to the dynamic aperture to represent it.

Two objectives usually adopted as probes are the injection efficiency and the beam's resilience to dipolar perturbations. The former is quite self-explanatory: the larger the dynamic aperture, the larger space for the beam to be captured during injection, and thus the larger the injection efficiency. The latter is related to the DA by the following: the larger the horizontal dipolar kicks the beam can survive, the larger the orbit distortions towards the positive or negative horizontal plane (depending on the kick direction). So the larger the amplitudes the beam explores as it oscillates, probing the DA borders. If the beam survives to large kicks, it means the ring can accomodate larger orbit distortions because of an increased dynamic aperture .

In summary, the dynamic aperture optimization procedure must consist on the exploration of sextupole (knobs) configurations yielding the largest dynamic aperture as accessed by as objective function such as injection efficiency or beam kick-resiliency.

4.2.1 Injection scheme for acummulation at SIRIUS storage ring

Beam acummulation into the storage ring occurs in the off-axis scheme. The beam is delivered at $x \approx -8$ mm, and receives the kick from the nonlinear kicker field. The field profile is nonlinear, with zero field and gradient at the center of the axis, so that it does not disturbs the stored beam. In the off-axis scheme, a sufficiently large dynamic aperture is desired to allow the beam to be captured into the storage ring. The predicted efficiency for SIRIUS setup, considering a dynamic aperture reaching $x = -9$ mm, was nearly 100%. What was observed during 2022 was an injection efficiency of about $88 \pm 8\%$.

4.3 Selection of optimization knobs

The dynamic aperture is determined by the quality of the dynamics in terms of perturbations and nonlinearities. Considering corrected quadrupoles and dipoles (linear optics), the main factors influencing SIRIUS DA are the nonlinearities introduced by the sextupoles and possbibly their field's small errors and deviations from the design parameters. The goal, thus, is to search for the sextupole configurations rendering the largest DA.

The sextupoles are the parmeters which can be tuned, the knobs. SIRIUS has 21 sextupole families: magnets powered by the same power supply. 6 of them are achromatic sextupoles. They are placed where the the dispersion is zero. The 15 other families are chromatic families. Table 4.1 shows the 21 sextupole families names. In

Table 4.1: SIRIUS sextupole families

achromatic	SFA0, SDA0, SFB0, SDB0, SDP0, SFP0
chromatic	SDA1, SFA1, SDA2, SFA2, SDA3, SDB1, SFB1 SDB2, SFB2, SDB3, SFP1, SDP1, SDP2, SFP2 SDP3

principle, thus, the optimization parameter space is 21-dimensional. In reality, we would like to change sextupoles without changing chromaticity. Since we need at least one degree of freedom for correcting chromaticity in the horizontal plane and one degree of freedom for correcting the chromaticity in vertical plane, there are 19 available knobs. The dimensionality of the search space can be further reduced by imposing additional constraints to certain families variations. The specific choices of knobs for optimzation experiments are discussed in more details in the Results section.

4.3.1 Characterization of Sextupole Magnets Configurations

Once a configuration of sextupoles (position in parameter space) is found, the nonlinear optics it provides the machine needs to be characterized. The characterizations consisted on evaluatig/measuring the followint figures of merit and desired features

- Injection efficiency in nominal off-axis conditions : this is the most desired characteristic. The sextupoles are to be optimized so the DA and the off-axis injection efficiency increase.
- Beam Kick resilience: a small current of 2 mA, concentrated in a single bucket is stored in the ring. The beam is kicked by the horizontal dipole kicker, which instantly provides a dipolar perturbation leading the beam to be displaced in the horizontal direction. The current before and after the kick is recorded by a current monitor (DCCT) and allows for the calculation of the fraction of the beam lost as a consequence of the kick and the transverse displacement. The procedure is repeated

with progressively stronger kicks, and a curve of beam loss as a function of the kick can be constructed. The smaller the losses for larger kicks, the larger the resilience.

- Phase portrait area: it is expected that the optimzation procedure increases the dynamic aperture of the machine, meaning it can accomodate larger oscillations and larger phase portraits $x - x'$. Using beam position monitors (BPMs) at the two ends of a straight section, which record the positions of the beam centroid at each turn, we can calculate the position and angle of the beam in the middle of the straight section, and thus recostruct the phase-portrait from turn-by-turn (TbT) data.

- Beam lifetime: the lifetime at SIRIUS is dominated by losses due to electron-electron interactions leading to momentum transfers exceeding the energy/momentum acceptance (MA). Optimization of DA does not necessarily leads to improvements in the MA. If the MA is reduced, the rate at which the beam is lost can increase, reducing the total lifetime. It is desireble that the configurations found during DA otpimzation do not worsen the MA and beam lifetime considerably.

- Chromaticity: Sextupoles are introduced in the storage ring for correction of focusing chromatic aberretions. When changing the sextupole settings, it is desired to do so in such a manner that the chromaticity is unchanged. The methods for choosing the optimization knobs already take into account the need for keeping constant chromaticity. Still, after optimization is performed, we need to check whether chromaticity is unchanged.

The first two characterizations are quite similar to the two most immediate objective function candidates mentioned above. Indeed, in most nonlinear dynamics optimzation experiments, optimization using injection efficiency or kick resilience as objectives seemed to be completely interchangable. Improvements in injection efficiency necessarily led to improvements in kick resilience, and vice-versa. As shown in more details in the results section, for the SIRIUS storage ring this appears not to be the case. The configurations can be specialized to improvements solely on injection efficiency or solely to kick resilience. This feature was observed during the characterization of the optimized sextupole settings with respect to these two figures of merit.

Chapter 5

Experiments and Results

This section presents partial results from the optimzation experiments carried out up until now. The early experiments were performed in december 2022, and the latest have been happening since february 2023.

5.0.1 Kick resilience optimization - december 2022

The parameter space (knobs) adopted consisted on the SDA0, SDB0, SDP0, SFA0, SFB0, SFP0, SDA1, SDB1, SDP1, SDA3, SDB3, SDP3, SFA1, SFB1, SFP1 sextupole families. The SDA2, SDB2, SDP2 and SFA2, SFB2, SFP2 families were used keep chromaticity constant when varying the optimization knobs. This was implemented in the following manner: RCDS freely proposed strength variations to the knob families. For each proposed change in strength, the corresponding changes in chromaticity were estimated from a chromaticity jacobian matrix constructed from the model. To the “correction" families were applied the strengths needed to cancel these chromaticity changes. In this first attempt, we tested the optimization routine twice, with different objective functions to probe the dynamic aperture.

- Objective function: kick resilience
  The first objective function adopted was the beam loss after dipolar kick from the horizontal dipole kicker. The idea was to minimize the loss at a given kick, and progressively increase the kicks, to probe larger acceptances. The BPMs acquisition was fired in synchrony with the dipole kick and beam-loss was calculated by comparing the sum-signal[1] of the beam's first 10 turns with the sum-signal of the last 10 turns. As for the strength of the dipole kick, we set a horizontal kick of $\Delta x' = -0.760$ mrad, which rendered about 35 - 40% of beam-loss.

- Experiment:
  With the aforementioned scheme for changing strengths in the sextupole families, RCDS was started to minimize the beam-loss upon the horizontal kick. In the

[1]BPMs determine the relative changes in position of the beam centroid from the differential image charges the beam induces in the device's four antennas. The sum-sginal consists on the sum of the signal from all the antennas and, up to a scale, represents the total beam current. Relative changes in sum-signal correspond to relative changes in beam current.

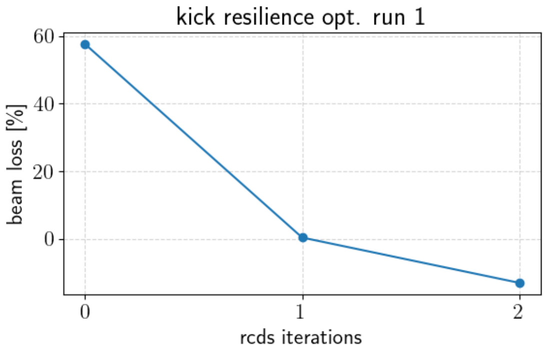

Figure 5.1: Objective function history vs. iterations of the first trial at beam-loss optimization.

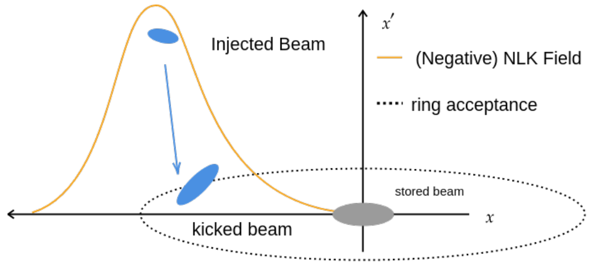

Figure 5.2: Injection conditions for DA optimization

algorithm's first iteration[2], beam loss dropped from 60% to nearly 0% (Figure 5.1). In the beginning of the 2nd iteration, the objective function took negative values (an artifact) and we stopped the optimization run.

- Results:
  The beam-loss minimization significantly improved the beam's resiliency to dipole kicks. After the optimization, it was necessary to kick the beam at approximately $\Delta x' = -0.850$ mrad to achieve the same 30–40% beam-loss rate previously achieved by a $\Delta x' = -0.760$ mrad kick. By the end of this first attempt, the machine magnets were cycled[3] and the configurations found during optimization were loaded. When trying to inject in the nominal off-axis scheme, the efficiency was quite low. The improved kick resilience, however, was preserved. This raised the suspicion that the aperture along the negative horizontal direction might have been negatively impacted by the procedure, while the aperture in x' increased. This observation motivated the adoption of injection efficiency to probe the DA.

5.0.2 Injection efficiency optimization - december 2022

The first attempt at optimizing DA by minizing beam-loss revealed that the optimization procedure did not improve injection efficiency. We started another attempt, using the injection efficiency itself as objective function. The knobs (parameter space) used were the same as in the beam-loss optimization.

- Objective function & setup:
  The off-axis injection efficiency was worsened by reducing the NLK strength so the

[2] An RCDS iteration is reached upon completing the one-dimensional optimization along all directions in the parameter space. After each iteration, the algorithm constructs a new (conjugate) direction according to Powell's method and may replace existing directions by this new conjugate direction.

[3] Cycling or standardizing magnets cosnsists on driving their power suplies with decaying sinusoidal waveforms to remove hysteresis effects and bring the magnets yokes to their standard reference magnetization.

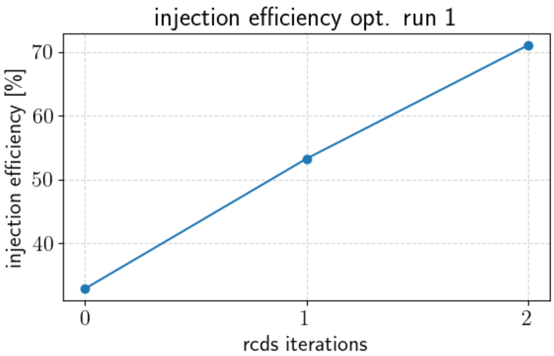

Figure 5.3: Objective function vs iterations during the first run of injection efficiency optimization

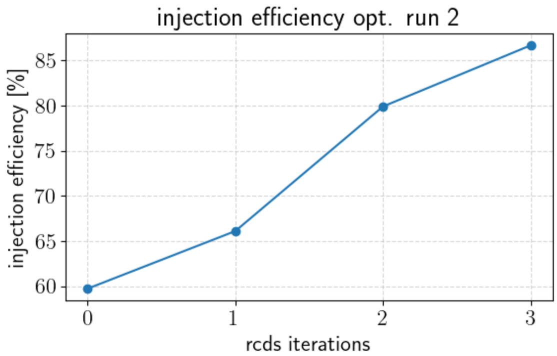

Figure 5.4: Objective function vs iterations during the second run of injection efficiency optimization

beam was injected in the upper-left border of the (x, x') aperture (see Figure 5.2). The efficiency under such conditions was about 30%. The maximization of injection efficiency under such injection conditions should correspond to a maximization of the DA evenly among the x and x' directions, as opposed to the increase on the x' direction only, as seemed to be the case in the previous attempt.

- Experiment:
  In the first run, within three iterations the injection efficiency reached 70%, as shown by Fig. 5.3. The algorithm stopped as it reached the maximum number of the objective function evaluations. A second run was launched, starting from the sextupole configurations just found in the first ruun. In four iterations, 85% efficiency was reached, as Fig. 5.4 shows.

- Results:
  When the NLK strength was restored to the reference value, meaning the nominal off-axis injection conditions were restored (in which the beam "lands" not at the border but within the acceptance), the injection efficiency fluctuated around 95–100% with good repeatability. There was a severe reduction in beam lifetime by the end of the last optimization trial. Measurement indicated 54.12 hrs lifetime at 15 mA current, while, the reference (non-optimized) configuration, lifetime at this same current is about 68 hrs.

We carried out chromaticity measurements in the machine loaded with the reference configuration (ref-config) and with the sextupole configurations found at iterations 0, 2, and 3 of the last injection efficiency optimization run (run shown by Fig. 5.4). Table 5.1 presents the measured values, from which we can note the chromaticity changes despite the efforts to anticipate and compensate them when applying changes to the sextupoles. It was later realized, due to the success of the optimization experiments throughout 2023, that the undesired changes in chromaticity are probably not related to this compensation scheme itself, but rather by the choice of sextupole families operating close to their saturation strengths. Under such conditions, the applied fields are not repeatable, and the excited fields might not correspond to the correct values required to control chromaticity.

machine configuration	ξ_x	ξ_y
ref-config	2.33 ± 0.02	2.531 ± 0.008
iter 0	2.59 ± 0.02	3.700 ± 0.008
iter 2	2.72 ± 0.04	3.704 ± 0.008
iter 3	2.76 ± 0.05	3.510 ± 0.01

Table 5.1: Chromaticity measurements for ref-config and sextupole configs. found at the second round of injection optimization

In summary, in these early attempts in december 2022 it was realized that beam-loss minimization/kick resilience maximization does not necessarily leads to injection efficiency improvements. The $x - x'$ phase space seems to be "elastic" and the dynamic aperture can be deformed preferably along x or x' directions, rather than being uniformily increased, as the experiences in other accelerators suggests.

The injection efficiency optimization was successful, but at the expense of a significant decrease in beam lifetime. Undesired chromaticity changes were also observed.

5.0.3 Optimization experiments throughout 2023

In 2023, optimzation experiments were carried in the machine configurations with the nominal tunes $(\nu_x, \nu_y) = (49.08, 14.14)$, Working Point 1, as well as in the $(49.20, 14.25)$ and $(49.16, 14.22)$ tunes, Working Points 2 and 3 (WPs 1, 2, 3). Results reported here have also been presented in Ref. [?] (on WPs 1 and 2) and on the presentation delivered at the Optics Tuning and Corrections for Future Colliders Workshop.

The major differences from the previous experiments consisted on

- the use of the average injection efficiency of 5 injection pulses at 2 Hz objective function to reduce the experimental noise sigma from $\sigma = \pm 8\%$ to $\pm 1\%$.
- Families SFP1 and SFB1 were not used as knobs in the otpimzation experiments since they operate close to their saturation strengthts, where hysteresis effects become significant.
- Knobs selection was based in choosing linear combinations spanning null space of the chromaticity response matrix for Working Points 1 and 2. See Ref. [?] for details. Working Point 3 knobs were chosen as described in section 9.1.

Optimization in Working Point 1

Three configurations were found, which resulted from optimizing the objective, loading the best configuration found and continuing the optimzation from the previous run's best.

For each one of the best configurations found during runs 1, 2 and 3 and also for the non-optimized reference configuration (ref. config.), turn-by-turn (TbT) BPM data of the stored beam kicked with the horizontal dipolar kicker were acquired. The DCCT current monitor allowed the determination of the current losses as a function of the horizontal kicks, which is shown by Figure 5.5. TbT data also allowed for the reconstruction of the (x, x') phase space of the beam under the influence of the kicks. Using two BPMs at the ends of an empty ID straight section, the position and angle of the beam were determined at each turn. Figure 5.7 shows the measured phase spaces for the ref. config. and the best configurations found during run 1, 2, and 3, at the fifth straight section (SA05), which is a high-beta section with identical optics to the injection point. In the measurement, the beam was under the influence of kicks rendering approximately the same current loss of 12%.

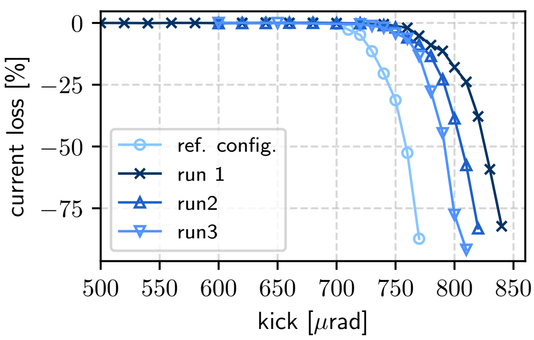

Figure 5.5: Current losses vs. horizontal dipole kick for the ref. config. and for the RCDS solutions at WP 1.

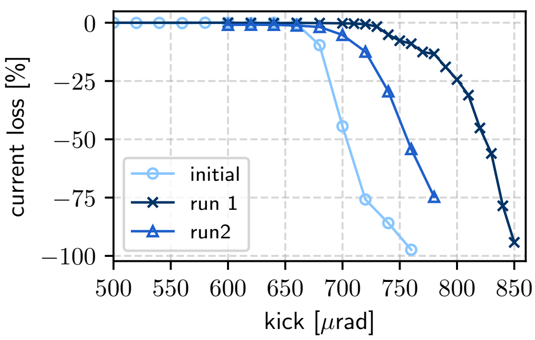

Figure 5.6: Current losses vs. horizontal dipole kick for the initial configuration and the RCDS solutions at WP 2.

Table 5.2 compiles the injection efficiencies (IE) achieved for each configuration during off-axis NLK injection in normal injection conditions ($x \approx -8.5$ mm, $x' \approx 0$). Again we stress that the point regarding the maleability of the phase portrait ellipses deformations: the configuration with the largest kick resilience, that of run 1, is not the one with the largest phase space area and IE performance. This could be explained if the phase space deformations of the ellipse at the kicker location for this sextupole setting resulted in a larger x'/x ratio, which would account for a larger kick acceptance and the worse injection performance compared to run 2.

Lifetime at 60 mA was measured at 20 hr for run 2 best configuration. Lifetime at the same conditions for the reference configuration is 21 hr. No significant chromaticity changes were observed: $(2.33, 2.53)$ in ref. config. vs. $(2.24, 2.39)$ in run 2 best solution.

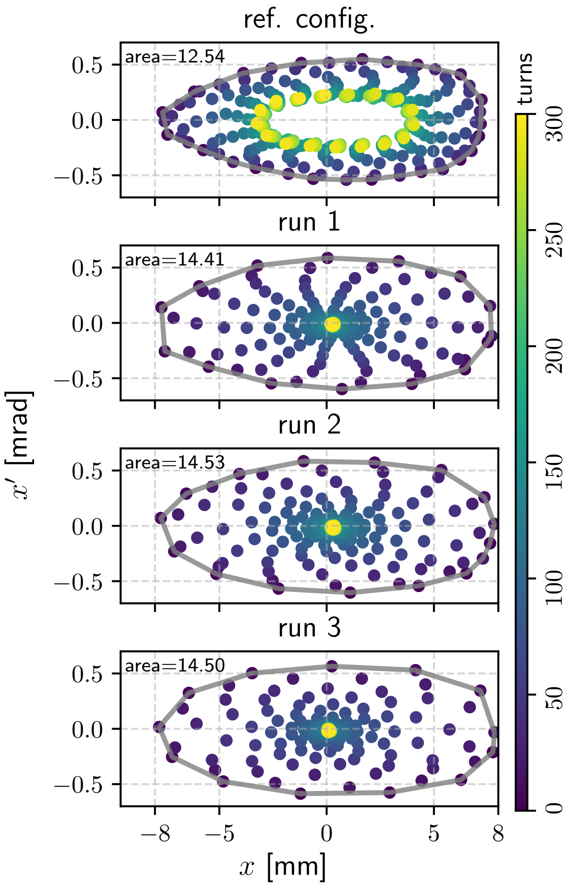

Figure 5.7: Measured phase space at SA05 high-beta straight section for the ref. config. and the best RCDS configurations of runs 1, 2 and 3 in WP 1. Color-map indicates the turns. The areas are in mm mrad. The beam was being kicked horizontally at 730 µrad in the ref. config, 790 µrad in run 1, 780 µrad in run 2, and 770 µrad, in run 3. Loss rates of 12%, 11%, 13% and 13%.

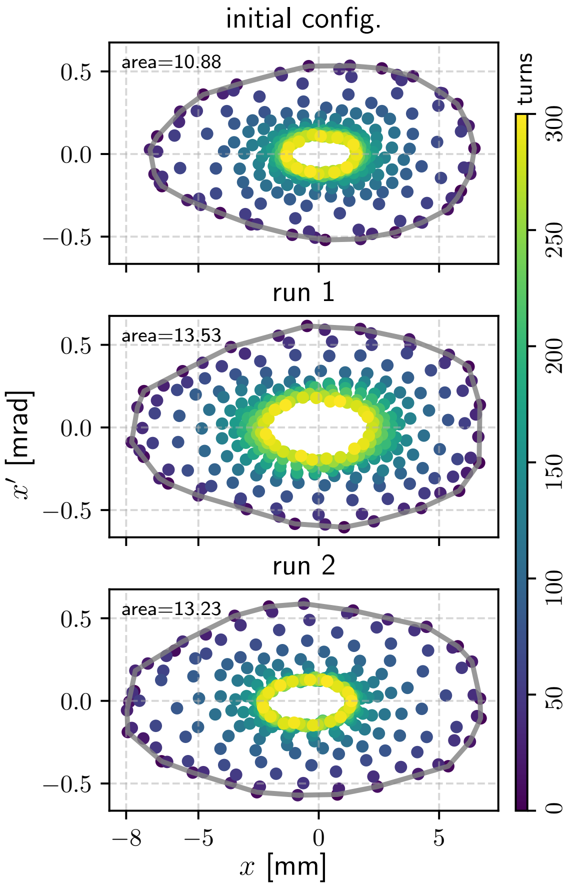

Figure 5.8: Measured phase space at SA05 high-beta straight section for the initial configuration and the best RCDS configurations of runs 1 and 2 in WP 2. Color-map indicates the turns. The areas are in mm mrad. The beam was being kicked horizontally at 680 µrad, for the initial configuration, 770 µrad for run 1, and at 720 µrad for run 2. Loss rates of 10%, 12% and 12%, respectively

Optimization in Working Point 2

In working point 2, two configurations were found: Run 1 and Run 2. The sextupoles were optimized from scratch from a configuration with the new tunes and then, from the best solution found, another round was launched.

TbT BPM data of the kicked stored beam in the initial configuration (non-optimzed) and in each run's best solution was acquired and allowed the determination of current losses vs. kicks, shown in Fig. 5.6, and the reconstruction of phase space, shown in Fig. 5.8. Table 5.2 compiles injection efficiencies achieved for the configurations in the new tunes during nominal off-axis injection. The configuration found during run 1 rendered the best IE, the largest kick resilience, a larger lifetime than the initial configuration (21 hrs, run 1 vs. 18 hrs, initial, at 60 mA), and the largest phase-space area increase.

Table 5.2: Injection efficiencies (IE) for configurations found for Working Points 1, 2 and 3.

working point 1		working point 2		working point 3	
configuration	IE [%]	configuration	IE [%]	configuration	IE [%]
ref. config.	88 ± 8	initial	51 ± 1	initial	
run 1	91 ± 1	run 1	79 ± 3	optimized	93 ± 3
run 2	98 ± 1	run 2	65 ± 1		
run 3	87 ± 3				

Optimization in Working Point 3

Two optimization runs were carried out, starting from sextupole settings of the reference configuration of the nominal tunes. Best configuration found at run 1 was loaded and run 2 was launched. The resulting configuration displayed injection efficiency of $93 \pm 3\%$ during nominal off-axis injection. Lifetime at 60 mA was measured at 19.5 hrs, so no significant reductions were observed.

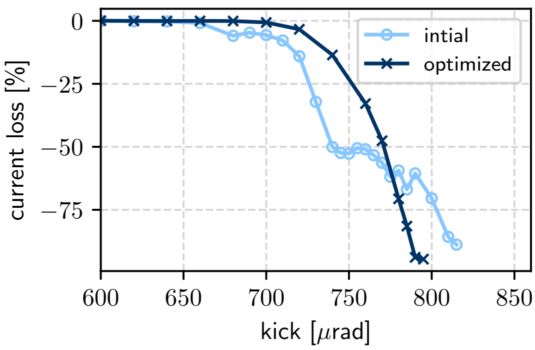

Figure 5.9: Current losses vs. horizontal dipole kick for the initial configuration and the RCDS solution at WP 3

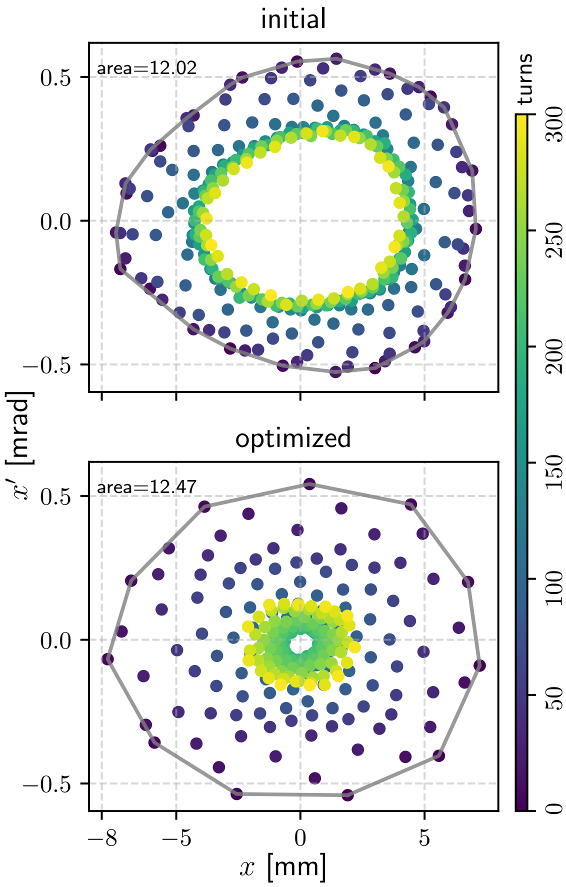

Figure 5.10: Measured phase space at SA05 high-beta straight section for the non-optimized configuration and the best RCDS configuration in WP 3. Color-map indicates the turns. The areas are in mm mrad.

Orbit stability improvements were confirmed by the orbit integrated spectrum density, which decreased by a factor of approximately 2 [?]. Orbit rms variations reached the record values of less than 1% of the horizontal beam size, in the horizontal plane, and less than 4% of the vertical beam size in the vertical plane.

In summary, in the experiments throughout 2023, the noise in the objective function was reduced and the injection efficiency average was established as the standard objective. No significant chromaticity changes were observed during/after the optimization runs, nor significant changes to beam lifetime, compared to the nominal working point reference configuration.

Excellent configurations were found in WP1, with 98% injection efficiency, but we still believe there is room for further improvements in the higher tunes configurations.

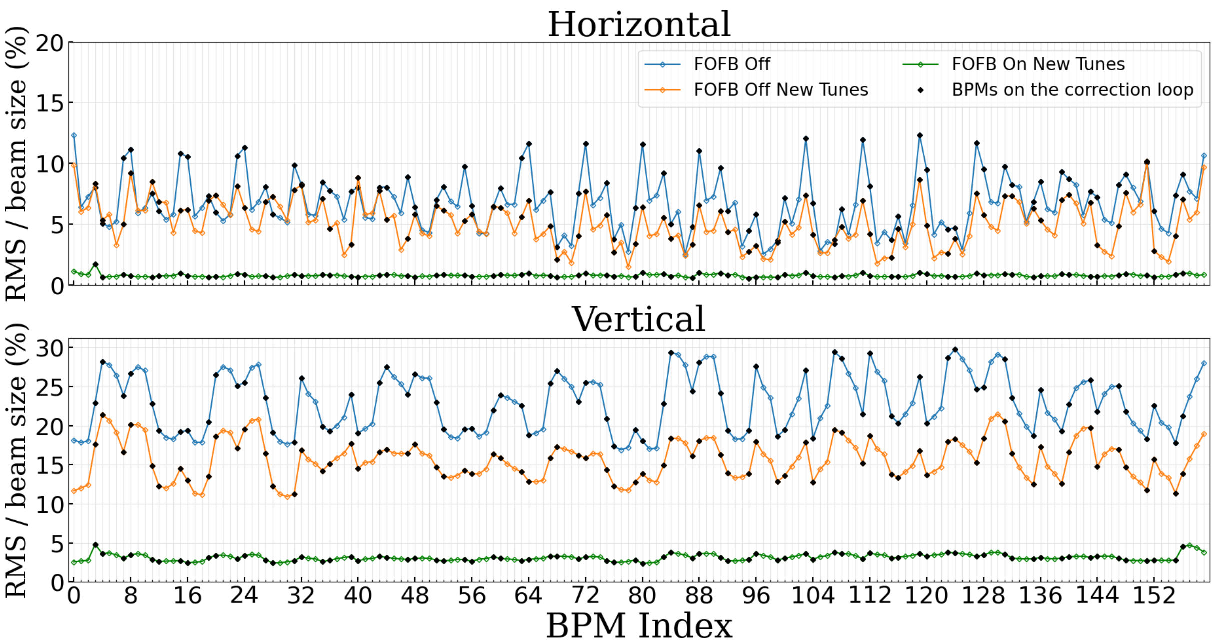

Figure 5.11: Horizontal/Vertical RMS orbit variations in units of the horizontal and vertical beam sizes. Blue curves represents variations in the nominal working point, WP1, orange curves are the orbit variations at WP3, and green curves variations at WP3 plus results of the recent improvements in Fast Orbit Feedback System. From [?]

5.1 Conclusions

The MSc. project is being developed on shcedule and should be completed within the stipulated duration of the grant. In the reported period from August 2022 to July 2023 the student has completed the graduate program requierements for course credits, co-athoured and collaborated in the writing of computer code for performing machine experiments, participated in the experiments and performed all the analysis of the obtained data. The student has also co-authored and submitted contributions to IPAC'23, the largest conference in the field of particle accelerators, and presented the results achieved so far during the project in the Optics Tuning and Corrections for Future Colliders Workshop, at CERN.

The work developed alongside the LNLS Accelerator Physics Group has contributed to the recent achievements of record orbit stability at the SIRIUS storage ring.

More experiments for further optimzation, exploration of working points and and characterizations of nonlinear dynamics performance should proceed in the upcoming months up until the end of the year, when the student should then focus in the writing of his dissertation.

Chapter 6

Discussion and Conclusions

Bibliography

[1] Huang, X. *Beam-based Correction and Optimization for Accelerators* (CRC Press, 2019). Google-Books-ID: y0PBDwAAQBAJ.

[2] Wolski, A. *Beam Dynamics In High Energy Particle Accelerators* (World Scientific, 2014). Google-Books-ID: 8c63CgAAQBAJ.

[3] Wiedemann, H. *Particle Accelerator Physics*. Graduate Texts in Physics (Springer International Publishing, Cham, 2015). URL http://link.springer.com/10.1007/978-3-319-18317-6.

[4] Huang, Z. Brightness and Coherence of Synchrotron Radiation and FELs. *Free Electron Lasers* (2013).

[5] Hettel, R. Challenges in the Design of Diffraction-limited Storage Rings. *Proceedings of the 5th Int. Particle Accelerator Conf.* **IPAC2014**, 5 pages, 0.551 MB (2014). URL http://jacow.org/ipac2014/doi/JACoW-IPAC2014-MOXBA01.html. Artwork Size: 5 pages, 0.551 MB ISBN: 9783954501328 Medium: PDF Publisher: JACoW Publishing, Geneva, Switzerland.

[6] Simoulin, V. The synchrotron generations. *Revue francaise de sociologie* **57**, 503–528 (2016). URL https://www.cairn-int.info/article-E_RFS_573_0503--the-synchrotron-generations.htm. Bibliographie_available: 1 Cairndomain: www.cairn-int.info Cite Par_available: 1 Publisher: Presses de Sciences Po.

[7] Liu, L. & Jr, H. W. Towards Diffraction Limited Storage Ring Based Light Sources (2017).

[8] Liu, L., Neuenschwander, R. T. & Rodrigues, A. R. D. Synchrotron radiation sources in Brazil. *Philosophical Transactions of the Royal Society A* (2019). URL https://royalsocietypublishing.org/doi/10.1098/rsta.2018.0235. Publisher: The Royal Society Publishing.

[9] Liu, L. *et al.* Status of Sirius Operation. *Proceedings of the 13th International Particle Accelerator Conference* **IPAC2022**, 4 pages, 0.882 MB (2022). URL https://jacow.org/ipac2022/doi/JACoW-IPAC2022-TUPOMS002.html. Artwork Size: 4 pages, 0.882 MB ISBN: 9783954502271 Medium: PDF Publisher: JACoW Publishing, Geneva, Switzerland.

[10] Liu, L., Oliveira, A. & Tavares, D. Status of SIRIUS operation with users (2022).

[11] Liu, L., Resende, X. R. & Rodrigues, A. R. D. Injection Dynamics for Sirius Using a Nonlinear Kicker 3 (2016).

[12] de Sá, F. H., Liu, L. & Resende, X. R. Optimization of Nonlinear Dynamics for Sirius (2016).

[13] Dester, P. S., Sá, F. H. & Liu, L. Energy acceptance and on momentum aperture optimization for the Sirius project. *Journal of Physics: Conference Series* **874**, 012068 (2017). URL https://doi.org/10.1088/1742-6596/874/1/012068. Publisher: IOP Publishing.

[14] Lee, S.-Y. *Accelerator Physics* (World Scientific, 2004). Google-Books-ID: VTc8Sdld5S8C.

[15] Landau, L. D. L. E. M. *The Classical Theory of Fields: Volume 2* (Butterworth-Heinemann, 1975). Google-Books-ID: X18PF4oKyrUC.

[16] Sands, M. The Physics of Electron Storage Rings: An Introduction. *Conf. Proc. C* **6906161**, 257–411 (1969).

Appendix A

Proof of the necessary condition for vectors conjugacy

Lorem ipsum dolor sit amet, consectetuer adipiscing elit. Ut purus elit, vestibulum ut, placerat ac, adipiscing vitae, felis. Curabitur dictum gravida mauris. Nam arcu libero, nonummy eget, consectetuer id, vulputate a, magna. Donec vehicula augue eu neque. Pellentesque habitant morbi tristique senectus et netus et malesuada fames ac turpis egestas. Mauris ut leo. Cras viverra metus rhoncus sem. Nulla et lectus vestibulum urna fringilla ultrices. Phasellus eu tellus sit amet tortor gravida placerat. Integer sapien est, iaculis in, pretium quis, viverra ac, nunc. Praesent eget sem vel leo ultrices bibendum. Aenean faucibus. Morbi dolor nulla, malesuada eu, pulvinar at, mollis ac, nulla. Curabitur auctor semper nulla. Donec varius orci eget risus. Duis nibh mi, congue eu, accumsan eleifend, sagittis quis, diam. Duis eget orci sit amet orci dignissim rutrum.

Nam dui ligula, fringilla a, euismod sodales, sollicitudin vel, wisi. Morbi auctor lorem non justo. Nam lacus libero, pretium at, lobortis vitae, ultricies et, tellus. Donec aliquet, tortor sed accumsan bibendum, erat ligula aliquet magna, vitae ornare odio metus a mi. Morbi ac orci et nisl hendrerit mollis. Suspendisse ut massa. Cras nec ante. Pellentesque a nulla. Cum sociis natoque penatibus et magnis dis parturient montes, nascetur ridiculus mus. Aliquam tincidunt urna. Nulla ullamcorper vestibulum turpis. Pellentesque cursus luctus mauris.

Nulla malesuada porttitor diam. Donec felis erat, congue non, volutpat at, tincidunt tristique, libero. Vivamus viverra fermentum felis. Donec nonummy pellentesque ante. Phasellus adipiscing semper elit. Proin fermentum massa ac quam. Sed diam turpis, molestie vitae, placerat a, molestie nec, leo. Maecenas lacinia. Nam ipsum ligula, eleifend at, accumsan nec, suscipit a, ipsum. Morbi blandit ligula feugiat magna. Nunc eleifend consequat lorem. Sed lacinia nulla vitae enim. Pellentesque tincidunt purus vel magna. Integer non enim. Praesent euismod nunc eu purus. Donec bibendum quam in tellus. Nullam cursus pulvinar lectus. Donec et mi. Nam vulputate metus eu enim. Vestibulum pellentesque felis eu massa.

Quisque ullamcorper placerat ipsum. Cras nibh. Morbi vel justo vitae lacus tincidunt ultrices. Lorem ipsum dolor sit amet, consectetuer adipiscing elit. In hac habitasse platea dictumst. Integer tempus convallis augue. Etiam facilisis. Nunc elementum fermentum wisi. Aenean placerat. Ut imperdiet, enim sed gravida sollicitudin, felis odio placerat quam, ac pulvinar elit purus eget enim. Nunc vitae tortor. Proin tempus nibh sit amet nisl. Vivamus quis tortor vitae risus porta vehicula.

Fusce mauris. Vestibulum luctus nibh at lectus. Sed bibendum, nulla a faucibus semper, leo velit ultricies tellus, ac venenatis arcu wisi vel nisl. Vestibulum diam. Aliquam pellentesque, augue quis sagittis posuere, turpis lacus congue quam, in hendrerit risus eros eget felis. Maecenas eget erat in sapien mattis porttitor. Vestibulum porttitor. Nulla facilisi. Sed a turpis eu lacus commodo facilisis. Morbi fringilla, wisi in dignissim interdum, justo lectus sagittis dui, et vehicula libero dui cursus dui. Mauris tempor ligula sed lacus. Duis cursus enim ut augue. Cras ac magna. Cras nulla. Nulla egestas. Curabitur a leo. Quisque egestas wisi eget nunc. Nam feugiat lacus vel est. Curabitur consectetuer.

Suspendisse vel felis. Ut lorem lorem, interdum eu, tincidunt sit amet, laoreet vitae, arcu. Aenean faucibus pede eu ante. Praesent enim elit, rutrum at, molestie non, nonummy vel, nisl. Ut lectus eros, malesuada sit amet, fermentum eu, sodales cursus, magna. Donec eu purus. Quisque vehicula, urna sed ultricies auctor, pede lorem egestas dui, et convallis elit erat sed nulla. Donec luctus. Curabitur et nunc. Aliquam dolor odio, commodo pretium, ultricies non, pharetra in, velit. Integer arcu est, nonummy in, fermentum faucibus, egestas vel, odio.

Sed commodo posuere pede. Mauris ut est. Ut quis purus. Sed ac odio. Sed vehicula hendrerit sem. Duis non odio. Morbi ut dui. Sed accumsan risus eget odio. In hac habitasse platea dictumst. Pellentesque non elit. Fusce sed justo eu urna porta tincidunt. Mauris felis odio, sollicitudin sed, volutpat a, ornare ac, erat. Morbi quis dolor. Donec pellentesque, erat ac sagittis semper, nunc dui lobortis purus, quis congue purus metus ultricies tellus. Proin et quam. Class aptent taciti sociosqu ad litora torquent per conubia nostra, per inceptos hymenaeos. Praesent sapien turpis, fermentum vel, eleifend faucibus, vehicula eu, lacus.

Pellentesque habitant morbi tristique senectus et netus et malesuada fames ac turpis egestas. Donec odio elit, dictum in, hendrerit sit amet, egestas sed, leo. Praesent feugiat sapien aliquet odio. Integer vitae justo. Aliquam vestibulum fringilla lorem. Sed neque lectus, consectetuer at, consectetuer sed, eleifend ac, lectus. Nulla facilisi. Pellentesque eget lectus. Proin eu metus. Sed porttitor. In hac habitasse platea dictumst. Suspendisse eu lectus. Ut mi mi, lacinia sit amet, placerat et, mollis vitae, dui. Sed ante tellus, tristique ut, iaculis eu, malesuada ac, dui. Mauris nibh leo, facilisis non, adipiscing quis, ultrices a, dui.

Morbi luctus, wisi viverra faucibus pretium, nibh est placerat odio, nec commodo wisi enim eget quam. Quisque libero justo, consectetuer a, feugiat vitae, porttitor eu, libero. Suspendisse sed mauris vitae elit sollicitudin malesuada. Maecenas ultricies eros sit amet ante. Ut venenatis velit. Maecenas sed mi eget dui varius euismod. Phasellus aliquet volutpat odio. Vestibulum ante ipsum primis in faucibus orci luctus et ultrices posuere cubilia Curae; Pellentesque sit amet pede ac sem eleifend consectetuer. Nullam elementum, urna vel imperdiet sodales, elit ipsum pharetra ligula, ac pretium ante justo a nulla. Curabitur tristique arcu eu metus. Vestibulum lectus. Proin mauris. Proin eu nunc eu urna hendrerit faucibus. Aliquam auctor, pede consequat laoreet varius, eros tellus scelerisque quam, pellentesque hendrerit ipsum dolor sed augue. Nulla nec lacus.

Suspendisse vitae elit. Aliquam arcu neque, ornare in, ullamcorper quis, commodo eu, libero. Fusce sagittis erat at erat tristique mollis. Maecenas sapien libero, molestie et, lobortis in, sodales eget, dui. Morbi ultrices rutrum lorem. Nam elementum ullamcorper leo. Morbi dui. Aliquam sagittis. Nunc placerat. Pellentesque tristique sodales est. Maecenas imperdiet lacinia velit. Cras non urna. Morbi eros pede, suscipit ac, varius vel, egestas non, eros. Praesent malesuada, diam id pretium elementum, eros sem dictum tortor, vel consectetuer odio sem sed wisi.

Appendix B

Algorithms Pseudocode

Lorem ipsum dolor sit amet, consectetuer adipiscing elit. Ut purus elit, vestibulum ut, placerat ac, adipiscing vitae, felis. Curabitur dictum gravida mauris. Nam arcu libero, nonummy eget, consectetuer id, vulputate a, magna. Donec vehicula augue eu neque. Pellentesque habitant morbi tristique senectus et netus et malesuada fames ac turpis egestas. Mauris ut leo. Cras viverra metus rhoncus sem. Nulla et lectus vestibulum urna fringilla ultrices. Phasellus eu tellus sit amet tortor gravida placerat. Integer sapien est, iaculis in, pretium quis, viverra ac, nunc. Praesent eget sem vel leo ultrices bibendum. Aenean faucibus. Morbi dolor nulla, malesuada eu, pulvinar at, mollis ac, nulla. Curabitur auctor semper nulla. Donec varius orci eget risus. Duis nibh mi, congue eu, accumsan eleifend, sagittis quis, diam. Duis eget orci sit amet orci dignissim rutrum.

Nam dui ligula, fringilla a, euismod sodales, sollicitudin vel, wisi. Morbi auctor lorem non justo. Nam lacus libero, pretium at, lobortis vitae, ultricies et, tellus. Donec aliquet, tortor sed accumsan bibendum, erat ligula aliquet magna, vitae ornare odio metus a mi. Morbi ac orci et nisl hendrerit mollis. Suspendisse ut massa. Cras nec ante. Pellentesque a nulla. Cum sociis natoque penatibus et magnis dis parturient montes, nascetur ridiculus mus. Aliquam tincidunt urna. Nulla ullamcorper vestibulum turpis. Pellentesque cursus luctus mauris.

Nulla malesuada porttitor diam. Donec felis erat, congue non, volutpat at, tincidunt tristique, libero. Vivamus viverra fermentum felis. Donec nonummy pellentesque ante. Phasellus adipiscing semper elit. Proin fermentum massa ac quam. Sed diam turpis, molestie vitae, placerat a, molestie nec, leo. Maecenas lacinia. Nam ipsum ligula, eleifend at, accumsan nec, suscipit a, ipsum. Morbi blandit ligula feugiat magna. Nunc eleifend consequat lorem. Sed lacinia nulla vitae enim. Pellentesque tincidunt purus vel magna. Integer non enim. Praesent euismod nunc eu purus. Donec bibendum quam in tellus. Nullam cursus pulvinar lectus. Donec et mi. Nam vulputate metus eu enim. Vestibulum pellentesque felis eu massa.

Quisque ullamcorper placerat ipsum. Cras nibh. Morbi vel justo vitae lacus tincidunt ultrices. Lorem ipsum dolor sit amet, consectetuer adipiscing elit. In hac habitasse platea dictumst. Integer tempus convallis augue. Etiam facilisis. Nunc elementum fermentum wisi. Aenean placerat. Ut imperdiet, enim sed gravida sollicitudin, felis odio placerat quam, ac pulvinar elit purus eget enim. Nunc vitae tortor. Proin tempus nibh sit amet nisl. Vivamus quis tortor vitae risus porta vehicula.

Fusce mauris. Vestibulum luctus nibh at lectus. Sed bibendum, nulla a faucibus semper, leo velit ultricies tellus, ac venenatis arcu wisi vel nisl. Vestibulum diam. Aliquam pellentesque, augue quis sagittis posuere, turpis lacus congue quam, in hendrerit risus eros eget felis. Maecenas eget erat in sapien mattis porttitor. Vestibulum porttitor. Nulla facilisi. Sed a turpis eu lacus commodo facilisis. Morbi fringilla, wisi in dignissim interdum, justo lectus sagittis dui, et vehicula libero dui cursus dui. Mauris tempor ligula sed lacus. Duis cursus enim ut augue. Cras ac magna. Cras nulla. Nulla egestas. Curabitur a leo. Quisque egestas wisi eget nunc. Nam feugiat lacus vel est. Curabitur consectetuer.

Suspendisse vel felis. Ut lorem lorem, interdum eu, tincidunt sit amet, laoreet vitae, arcu. Aenean faucibus pede eu ante. Praesent enim elit, rutrum at, molestie non, nonummy vel, nisl. Ut lectus eros, malesuada sit amet, fermentum eu, sodales cursus, magna. Donec eu purus. Quisque vehicula, urna sed ultricies auctor, pede lorem egestas dui, et convallis elit erat sed nulla. Donec luctus. Curabitur et nunc. Aliquam dolor odio, commodo pretium, ultricies non, pharetra in, velit. Integer arcu est, nonummy in, fermentum faucibus, egestas vel, odio.

Sed commodo posuere pede. Mauris ut est. Ut quis purus. Sed ac odio. Sed vehicula hendrerit sem. Duis non odio. Morbi ut dui. Sed accumsan risus eget odio. In hac habitasse platea dictumst. Pellentesque non elit. Fusce sed justo eu urna porta tincidunt. Mauris felis odio, sollicitudin sed, volutpat a, ornare ac, erat. Morbi quis dolor. Donec pellentesque, erat ac sagittis semper, nunc dui lobortis purus, quis congue purus metus ultricies tellus. Proin et quam. Class aptent taciti sociosqu ad litora torquent per conubia nostra, per inceptos hymenaeos. Praesent sapien turpis, fermentum vel, eleifend faucibus, vehicula eu, lacus.

Pellentesque habitant morbi tristique senectus et netus et malesuada fames ac turpis egestas. Donec odio elit, dictum in, hendrerit sit amet, egestas sed, leo. Praesent feugiat sapien aliquet odio. Integer vitae justo. Aliquam vestibulum fringilla lorem. Sed neque lectus, consectetuer at, consectetuer sed, eleifend ac, lectus. Nulla facilisi. Pellentesque eget lectus. Proin eu metus. Sed porttitor. In hac habitasse platea dictumst. Suspendisse eu lectus. Ut mi mi, lacinia sit amet, placerat et, mollis vitae, dui. Sed ante tellus, tristique ut, iaculis eu, malesuada ac, dui. Mauris nibh leo, facilisis non, adipiscing quis, ultrices a, dui.

Morbi luctus, wisi viverra faucibus pretium, nibh est placerat odio, nec commodo wisi enim eget quam. Quisque libero justo, consectetuer a, feugiat vitae, porttitor eu, libero. Suspendisse sed mauris vitae elit sollicitudin malesuada. Maecenas ultricies eros sit amet ante. Ut venenatis velit. Maecenas sed mi eget dui varius euismod. Phasellus aliquet volutpat odio. Vestibulum ante ipsum primis in faucibus orci luctus et ultrices posuere cubilia Curae; Pellentesque sit amet pede ac sem eleifend consectetuer. Nullam elementum, urna vel imperdiet sodales, elit ipsum pharetra ligula, ac pretium ante justo a nulla. Curabitur tristique arcu eu metus. Vestibulum lectus. Proin mauris. Proin eu nunc eu urna hendrerit faucibus. Aliquam auctor, pede consequat laoreet varius, eros tellus scelerisque quam, pellentesque hendrerit ipsum dolor sed augue. Nulla nec lacus.

Suspendisse vitae elit. Aliquam arcu neque, ornare in, ullamcorper quis, commodo eu, libero. Fusce sagittis erat at erat tristique mollis. Maecenas sapien libero, molestie et, lobortis in, sodales eget, dui. Morbi ultrices rutrum lorem. Nam elementum ullamcorper leo. Morbi dui. Aliquam sagittis. Nunc placerat. Pellentesque tristique sodales est. Maecenas imperdiet lacinia velit. Cras non urna. Morbi eros pede, suscipit ac, varius vel, egestas non, eros. Praesent malesuada, diam id pretium elementum, eros sem dictum tortor, vel consectetuer odio sem sed wisi.

Appendix C

Momentum Compaction Factor and the relation between energy deviations and RF frquency changes

Momentum compaction factor is the quantity characterizing the energy/momentum dependence of revolution time/frequency of orbits. The path length traversed by a particle reads up to first order reads

$$\mathrm{d}\ell = (1 + G(s)x)\mathrm{d}s \tag{C.1}$$

where $x(s) = x_\beta(s) + \eta(s)\delta$. For $\delta = 0$ we have simply

$$L = \oint (1 + G(s)x_\beta(s))\,\mathrm{d}s$$

thus the additional length traversed by an off-energy particle reads

$$\delta\ell = \oint G(s)\eta(s)\delta\,\mathrm{d}s \tag{C.2}$$

thus we can write

$$\frac{\delta\ell}{L} = \alpha\delta$$

by defining the *momentum compaction factor*:

$$\alpha = \frac{1}{L}\oint G(s)\eta(s)\,\mathrm{d}s \tag{C.3}$$

For relativistic electrons, the increase in energy leads to enlargement of orbits with neglible increase of velocity. Thus, the orbit revolution time decreases. This apparently paradoxical result.

$$\frac{\Delta T}{T} = \left(\alpha - \frac{1}{(v/c)^2\gamma^2}\right)\delta$$

where $\delta = \Delta E/E$. For $v \to c$, (large γ), we have

$$\frac{\Delta T}{T} = \alpha\frac{\Delta E}{E}$$

or, equivalently

$$\frac{\Delta f}{f} = -\alpha \frac{\Delta E}{E}$$

For non-relativistic electrons, the increase in energy leads to increase of velocity and the orbit time remains fixed. This is what makes cyclotrons possible.